



# Hydraulic traits explain differential responses of Amazonian forests to the 2015 El Niño-induced drought

Fernanda de V. Barros<sup>1</sup>\* D, Paulo R. L. Bittencourt<sup>1,2</sup>\*, Mauro Brum<sup>1</sup>\*, Natalia Restrepo-Coupe<sup>3,4</sup>, Luciano Pereira 1 D, Grazielle S. Teodoro 5 D, Scott R. Saleska 3, Laura S. Borma 6, Bradley O. Christoffersen 7 D, Deliane Penha<sup>8</sup>, Luciana F. Alves<sup>9</sup>, Adriano J. N. Lima<sup>10</sup>, Vilany M. C. Carneiro<sup>10</sup>, Pierre Gentine<sup>11</sup>, Jung-Eun Lee<sup>12</sup>, Luiz E. O. C. Aragão<sup>2,13</sup>, Valeriy Ivanov<sup>14</sup>, Leila S. M. Leal<sup>15</sup>, Alessandro C. Araujo<sup>16</sup> and Rafael S. Oliveira<sup>1</sup>

<sup>1</sup>Department of Plant Biology, Institute of Biology, CP 6109, University of Campinas UNICAMP, Campinas, SP 13083-970, Brazil; <sup>2</sup>College of Life and Environmental Sciences, University of Exeter, Exeter, EX4 4SB, UK; <sup>3</sup>Department of Ecology and Evolutionary Biology, University of Arizona, Tucson, AZ 85721, USA; <sup>4</sup>School of Life Science, University of Technology Sydney, Sydney, NSW 2006, Australia; <sup>5</sup>Instituto de Ciências Biológicas, Universidade Federal do Pará, Belém, PA 66075-110, Brazil; <sup>6</sup>Earth System Science Centre, National Institute for Space Research, Av. dos Astronautas, 1.758, São José dos Campos, SP 12227-010, Brazil; Department of Biology and School of Earth, Environmental and Marine Sciences, University of Texas Rio Grande Valley, Edinburg, TX 78539, USA; \*Society, Nature and Development Department, Federal University of Western Pará (UFOPA), Santarém, PA 68035-110, Brazil; \*Center for Pará (UFOPA), San Tropical Research, Institute of the Environment and Sustainability, University of California - Los Angeles, Los Angeles, CA 90095, USA; 10 Laboratório de Manejo Florestal, Instituto Nacional de Pesquisas na Amazônia - INPA, Manaus, AM 69.067-375, Brazil; 11 Department of Earth and Environmental Engineering, Columbia University, New York, NY 10027, USA; 12 Department of Earth and Planetary Sciences, Brown University Providence, 324 Brook Street, Providence, RI 02912, USA; 13 Remote Sensing Division, National Institute for Space Research, Av. dos Astronautas, 1.758, São José dos Campos, SP 12227-010, Brazil; 14Department of Civil and Environmental Engineering, University of Michigan, Ann Arbor, MI 48019, USA; 15Laboratory of Sustainable Systems Analyses, Oriental Amazon Embrapa, Belém, Pará 66083-156, Brazil; 16LBA Program Micrometeorology Group, INPA, Manaus, Amazonas 69.067-375, Brazil

Authors for correspondence: Fernanda de V. Barros Tel: +55 19 35916177 Email: nandavascon@gmail.com

Paulo R. L. Bittencourt Tel: +55 19 991331952 Email: paulo09d@gmail.com

Rafael S. Oliveira Tel: +55 19 988231042 Email: rafaelsoliv@gmail.com

Received: 14 December 2018 Accepted: 28 April 2019

New Phytologist (2019) doi: 10.1111/nph.15909

Key words: 2015-ENSO, Amazon tropical forest, drought, embolism resistance, hydraulic traits, plant functional diversity.

## **Summary**

- · Reducing uncertainties in the response of tropical forests to global change requires understanding how intra- and interannual climatic variability selects for different species, community functional composition and ecosystem functioning, so that the response to climatic events of differing frequency and severity can be predicted.
- Here we present an extensive dataset of hydraulic traits of dominant species in two tropical Amazon forests with contrasting precipitation regimes – low seasonality forest (LSF) and high seasonality forest (HSF) - and relate them to community and ecosystem response to the El Niño-Southern Oscillation (ENSO) of 2015.
- Hydraulic traits indicated higher drought tolerance in the HSF than in the LSF. Despite more intense drought and lower plant water potentials in HSF during the 2015-ENSO, greater xylem embolism resistance maintained similar hydraulic safety margin as in LSF. This likely explains how ecosystem-scale whole-forest canopy conductance at HSF maintained a similar response to atmospheric drought as at LSF, despite their water transport systems operating at different water potentials.
- · Our results indicate that contrasting precipitation regimes (at seasonal and interannual time scales) select for assemblies of hydraulic traits and taxa at the community level, which may have a significant role in modulating forest drought response at ecosystem scales.

### Introduction

Increases in the frequency and duration of climatic anomalies, such as drought events induced by the El Niño-Southern Oscillation (ENSO), are resulting in higher plant mortality, including in Amazonia, home of the world's largest contiguous tropical forests (Williamson et al., 2000; Phillips et al., 2010; Lintner

Most early ecosystem modelling studies used 'big leaf' approaches (in which whole forest responses are modelled after

et al., 2012; Fu et al., 2013). Amazon forests play a significant role in regional and global carbon and water cycles, and provide essential ecosystem services (Oyama & Nobre, 2003; Malhi et al., 2009; Davidson et al., 2011); many efforts thus seek to understand and predict how these forests respond to drought (Da Costa et al., 2010; Joetzjer et al., 2014; Brienen et al., 2015; Rowland et al., 2015).

<sup>\*</sup>These authors contributed equally to this work.

average growth responses of single plants or a small number of plants) that do not represent a diversity of functional strategies; these models tended to predict either large-scale catastrophic forest dieback (Cox et al., 2004; Good et al., 2011) or forest persistence (Friedlingstein et al., 2006; Cox et al., 2013; Huntingford et al., 2013). More recent models which account for diversity in functional growth strategies and landscape heterogeneity tend to simulate more nuanced resilience emerging from trait-based selection among growth strategies (Sakschewski et al., 2016) and more heterogeneous transitions (Levine et al., 2016). The inclusion of functional traits in models is therefore expected to improve simulations of forest drought vulnerability and resilience (Fisher et al., 2015; Gentine et al., 2016; Xu et al., 2016; Konings et al., 2017; Manoli et al., 2018).

Two empirical challenges confront efforts to improve such models: the need to increase knowledge of the composition of relevant functional traits of different systems (Medlyn *et al.*, 2016), and the need to test how such knowledge about functionally different individuals scales to ecosystem behaviour – the scale relevant to interactions with the atmosphere and regional climate. To address these challenges, we investigated two different tropical evergreen forests with contrasting climates and different species compositions by, first, characterizing their differences in terms of functional traits, and then by testing hypotheses for how functional differences would affect whole-ecosystem responses.

For functional diversity, we focus on hydraulic traits, particularly those related to embolism resistance, which are key to explaining such important factors as tree mortality, drought resistance and species distribution (Anderegg et al., 2015, 2016; Rowland et al., 2015; Oliveira et al., 2019). Embolism formation in the xylem decreases water supply to the leaves, forcing plants to reduce transpiration and, consequently, reducing photosynthesis and the energy available for physiological functions (Sperry et al., 2002; McDowell et al., 2008). The water potentials at which plant tissues (i.e. stem xylem) lose 50% or 88% of their conductance (P<sub>50</sub> or P<sub>88</sub>, respectively) are common measures of xylem embolism resistance (Tyree & Sperry, 1989; Sperry et al., 2002), while hydraulic safety margins to P<sub>50</sub> (HSM<sub>P50</sub>) – the difference between the minimum water potential measured in field conditions and P<sub>50</sub> -is a frequently used index of plant drought resistance (Meinzer et al., 2009). Hydraulic safety margins (e.g. HSM<sub>P50</sub>) are observed in the majority of sampled woody species around the globe to be maintained within a narrow range despite the large diversity of embolism resistance (quantified as P<sub>50</sub>), which generally increases as mean annual precipitation declines (Choat et al., 2012). Drought resistance is a key strategy affecting the distribution of species along water availability gradients, which act as environmental filters, including or excluding species based on their traits (Engelbrecht et al., 2005, 2007; Markesteijn et al., 2011; Esquivel-Muelbert et al., 2017; Oliveira et al., 2019).

For ecosystem-level behaviour, we focused on whole-forest canopy conductance ( $G_s$ ), an ecosystem-level trait that is both likely related to the hydraulic traits we are measuring, and which plays a central role in coupling ecosystems to the atmosphere. Critically, canopy conductance includes stomatal conductance (aggregated across all leaves in the canopy), which controls plant

water use and couples the plant water and carbon cycles (Collatz et al., 1991; Lin et al., 2015).

We ask whether different precipitation regimes in different Amazon forests lead to community-scale differences in hydraulic traits, and in vegetation responses to extreme drought events. To address this question, we studied hydraulic traits of dominant tree species in two evergreen tropical forest sites with contrasting rainfall regimes: a low seasonality forest (LSF) characterized by low seasonal and interannual rainfall variability in central Amazon (near Manaus, Brazil), and a high seasonal forest (HSF) with substantial seasonal and interannual precipitation variability in eastern Amazon (near Santarem, Brazil).

We then compared species-, community- and ecosystem-level responses at these two forests during a typical dry season period and during one of the most extreme drought El Niño events (referred to here as 2015-ENSO or just ENSO) ever recorded in Amazon rainforests (Jiménez-Muñoz *et al.*, 2016; Panisset *et al.*, 2018). We hypothesized that:

- 1 More variable precipitation regimes select for more drought-resistant communities. We predict dominant species in the HSF have traits associated with higher drought tolerance than the LSF.

  2 Communities in environments with higher precipitation variability are less sensitive to extreme drought events than communities in environments with lower precipitation variability. We estimated sensitivity as the change in water potential from a regular year dry season to the 2015-ENSO dry season. We predict that HSF species and the community are less sensitive to the 2015-ENSO than the LSF, and that embolism resistance modulates the magnitude of the response. Additionally, we hypothesize the species response to this El Niño event is mediated by their hydraulic traits.
- 3 Community-level water use responses to atmospheric and soil drought is less intense in forests with more variable precipitation. We predict ecosystem canopy conductance, a measure of plant community water use response to environment changes, is less sensitive to vapour pressure deficit and cumulative water deficit in HSF than in LSF.

To test these hypotheses, we combine a unique dataset of xylem embolism resistance, plant water potential (i.e. the physical driver of embolism formation) and canopy conductance in tropical forest species, in the novel context of a strong El Niño event. We propose an approach that allows us to scale species-level hydraulic traits to community-level properties, contributing to the critical overarching goal of linking individual plant trait composition to ecosystem level functioning.

### **Materials and Methods**

## Study sites

This study was carried out at two Large-Scale Biosphere–Atmosphere Experiment in Amazon forest (LBA) sites, with contrasting precipitation regimes. The low seasonality forest (LSF) is located in central Amazonia, at the Cuieras Biological Reserve (K34 site), near Manaus, Amazonas, Brazil (60°21′W, 2°61′S). The mean annual precipitation is *c.* 2400 mm, with 2 months of

dry season (precipitation < 100 mm) in July and August (Araujo et al., 2002; De Gonçalves et al., 2013). The higher seasonality forest (HSF) is located in the eastern Amazonia in the Tapajós National Forest (K67 site), near Santarém, Pará, Brazil (54°58'W, 2°51'S). It is drier than the Manaus region, with an annual mean precipitation of c. 1900 mm (Parrotta et al., 1995), a longer dry season (5 months, on average) and higher interannual climatic variability. Average annual vapour pressure deficit (VPD) at the HSF site is slightly higher than at LSF (means  $\pm$  SD of 0.94  $\pm$  0.3 kPa and 0.84  $\pm$  0.34 kPa, respectively), however dry season VPDs do not differ between the sites  $(1.05 \pm 0.18 \, \text{kPa})$  and  $1.08 \pm 0.26 \, \text{kPa}$ , for the HSF and LSF, respectively; Supporting Information Fig. S1). The LSF soils are characterized by tertiary sediments covered by clayey Oxisols on the plateaus and sandy Spodosols on the valley bottoms (Araujo et al., 2002), whereas the HSF soils are clayey Oxisols, deeply weathered, with no concretions or impeding layers, at least in the upper 12 m (Oliveira et al., 2005; Nepstad et al., 2007).

### Species selection

At each site, we selected locally and regionally abundant woody species or genera that contribute significantly to Amazon forest biomass (Ter Steege *et al.*, 2013; Fauset *et al.*, 2015). We studied 17 species in the LSF and nine in the HSF (Table S1; see Brum *et al.*, 2018), which correspond, respectively, to 13.7% and 35.0% of the total forest stem basal area. Embolism vulnerability curves were also measured for three additional species in the HSF (*Manilkara huberi, Tachigali chrysophylla* and *Minquartia guianensis*, representing 6.70%, 3.94% and 0.07% of total forest stem basal area).

The LSF and HSF sites differ in species richness, but mainly in terms of dominance homogeneity (Carneiro, 2004; Vieira et al., 2004; Longo, 2013), which led us to sample more species in the LSF to reach a minimum of 10% of forest stem basal area (Table S1). According to previous surveys, which used trees with stem diameter at breast height (DBH) > 10 cm, the species density at the LSF is c. 153.2 species ha<sup>-1</sup> (based on 3.5-ha sampling, measured on the plateaus with total basal area of 28.3 m<sup>2</sup> ha<sup>-1</sup>, Carneiro, 2004), while at the HSF the density was 133 species ha<sup>-1</sup> (4-ha transects sampling, Vieira *et al.*, 2004; with total basal area of 30.8 m<sup>2</sup> ha<sup>-1</sup>, Pyle et al., 2008 updated by Longo, 2013). The dominance in the LSF is more homogeneous, and the most dominant tree species (i.e. Eschweilera wachenheimii) represents 3.02% of total basal area, followed by a few species between 1% and 2% (Carneiro, 2004); whereas in the HSF, few species are locally hyperdominant (i.e. Erisma uncinatum, Chamaecrista xinguensis and Coussarea albescens, corresponding to 11.1%, 6.1% and 4.6% of the total basal area, respectively).

### Hydraulic traits

Xylem vulnerability to embolism was assessed by the relationship between the percentage loss of xylem conductivity (PLC) and xylem water potential ( $\Psi$ ). PLC was estimated from percentage air discharge (PAD) using the pneumatic method (Pereira *et al.*,

2016). To obtain these curves, we collected sun-exposed branches longer than 1 m in length early in the morning, from one to three individuals per tree species (Table S1) with DBH across species ranging from 2.7 to 98.0 cm. For some species, we sampled only one individual due to difficulties of access to very tall trees (e.g. > 35 m height). We cut a branch under water inside a bucket and covered it with a plastic bag overnight before measurements (following Oliveira et al., 2019 and Brum et al., 2018). To induce cavitation, we used the bench dehydration method (Sperry et al., 1988). Stem  $\Psi$  was measured as leaf  $\Psi$  after equilibrating the branch inside a black plastic bag for at least 1 h before making the measurement. We measured leaf  $\Psi$  (MPa) with a pressure chamber (PMS 1000; PMS Instruments Co., Albany, OR, USA). We calculated P50 and P88, defined as the water potentials at which the tissue loses 50% and 88% of its hydraulic conductivity, respectively, by fitting a sigmoidal function to the data (Pammenter & Vander Willigen, 1998):

$$PAD = \frac{100}{1 + exp\left(\frac{S_p}{25}\left(\psi_x - \psi_{p50}\right)\right)}$$

where PAD (percentage of air discharge) and  $\Psi_x$  (xylem water potential, MPa) are the measurement data, to which the parameters  $\Psi_{p50}$  (xylem water potential, when PAD equals 50%) and  $S_p$  (slope of the curve, % PAD MPa<sup>-1</sup>) were fitted.

The minimum leaf water potential  $(\Psi_{min})$  was measured during the peak of the dry season of an ENSO ( $\Psi_{ENSO}$ ) and non-ENSO ( $\Psi_{nonENSO}$ ) year. The  $\Psi_{nonENSO}$  was measured during the dry season in August 2016 and December 2014, for the LSF and HSF sites, respectively. The  $\Psi_{ENSO}$  was measured during the driest period of the ENSO event in October 2015 for the LSF and December 2015 for the HSF. The driest interval was determined frrom the cumulative water deficits for both sites (Fig. 1) (CMWD; see Microclimatic and soil data below). The leaf  $\Psi$  was measured with a pressure chamber in two or three leaves of the same individuals used to measure the vulnerability curves. Leaves were collected between 12:00 and 14:30 h from sun-exposed branches. For both sites, the water potential was collected over an interval of <7 d in each period (ENSO or non-ENSO). There were a few short and light rain events in the LSF during this sampling period, however they were insufficient to increase soil moisture. The water potential was always measured after at least 1 day without rain. In the HSF there was no rain during the months during which Ψ was measured.

Species hydraulic safety margins (HSM) with respect to  $P_{50}$  and  $P_{88}$  (HSM $_{P50}$  and HSM $_{P88}$ , respectively) were calculated as minimum leaf  $\Psi$  ( $\Psi_{nonENSO}$  and  $\Psi_{ENSO}$ ) minus  $P_{50}$ , or  $P_{88}$ , respectively. The HSM of the non-ENSO period is thus referred to as HSM $_{nonENSO}$  and that of the ENSO period, as HSM $_{ENSO}$ . We assumed that leaf  $\Psi$  was a suitable estimator of xylem  $\Psi$  in terminal branches.

### Wood anatomy

We collected wood samples from  $2^{nd}$  or  $3^{rd}$  order branches (diameter from c. 1 to 2 cm, i.e. the same as used for vulnerability curves) for

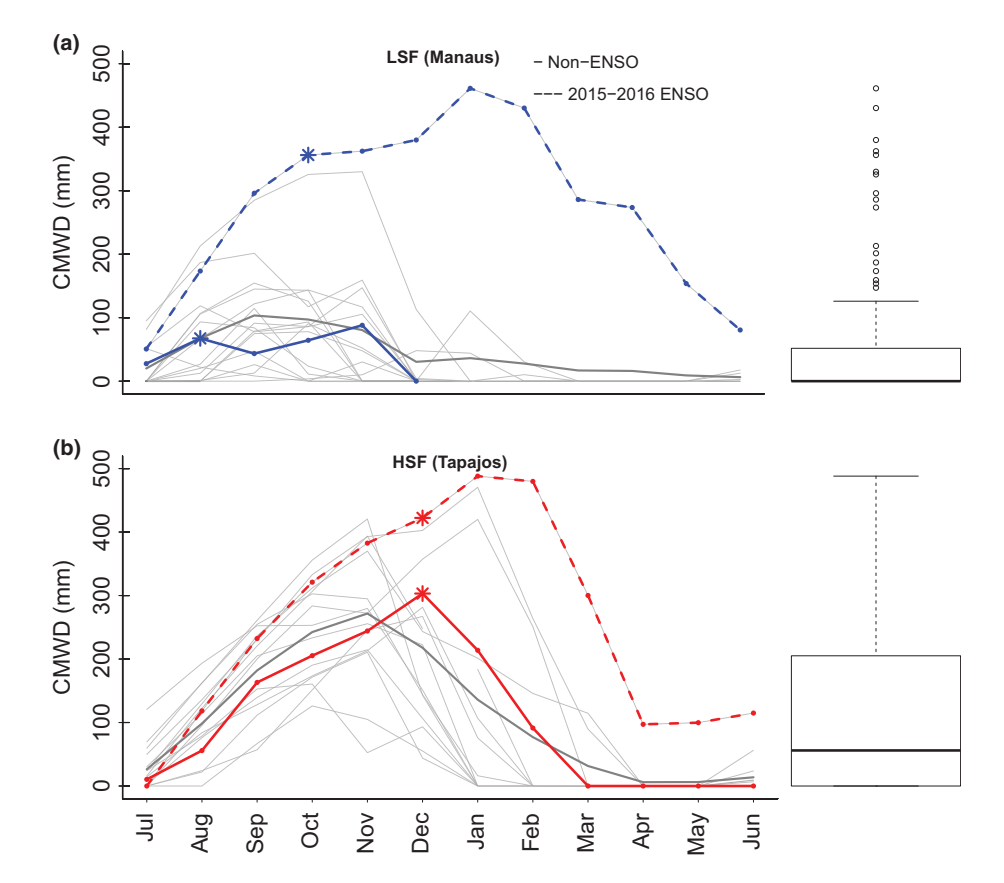


Fig. 1 Monthly cumulative water deficit (mm) from 1999 to 2016 for Manaus (a), and Tapajos (b). Blue and red lines correspond to the periods of water potential measurements at each site for LSF (low seasonal forest; Manaus) and HSF (high seasonal forest; Tapajós), respectively: the solid line represents the non-ENSO year (2014-2015 for Tapajós and 2016-2017 for Manaus), and the dashed line the 2015-2016 ENSO year. Grey lines represent all other years and the thick grey line is the mean across all years, including the ENSO year. Asterisks on blue and red lines denote the months during which the water potential data were collected. Boxplot inserts represent CMWD distribution for each site. Whiskers are either maximum/minimum value or, when outliers are present, 1.5 interquartile range above/below the quartiles 2 and 3.

anatomy. We kept the samples in formalin-acetic acid-alcohol (FAA) for a few days and then exchanged this for 50% alcohol to maintain the wood tissue integrity. We cut the samples using a manual microtome, dyed them with safranin and toluidine blue, and placed them on microscope slides. For each individual sample, we took photographs from three regions of different xylem slices (three per individual) using a digital camera (DP71; Olympus Corp., Tokyo, Japan) coupled to a polarizing microscope (Olympus BX51). The images were processed using IMAGE J software (v.1.6.0\_20) (Schneider et al., 2012). For each image, we measured the area of each vessel, the total vessel area (VA; mm<sup>2</sup> of vessel area per mm<sup>2</sup> of xylem area) and their density (VD; number of vessels per mm<sup>2</sup> of xylem area). We calculated effective vessel diameters from the area, assuming vessels were circular. From these data we calculated the vessel hydraulic diameter ( $D_h$ ;  $\mu$ m) and the theoretical specific hydraulic conductance of the xylem  $(K_h; kg MPa^{-1} s^{-1} m^{-1})$  using the Poiseuille Law (Scholz et al., 2013) as:

$$D_{\mathrm{h}} = \left(\sum_{1}^{\mathrm{n}} D_{\mathrm{i}}^{4}\right)^{\frac{1}{4}}$$

$$\mathit{K}_{h} = \left(\frac{\pi \rho}{128 \eta \mathit{A}}\right) \sum_{1}^{n} \mathit{D}_{i^{4}}$$

where  $D_i$  is each individual vessel diameter from 1 to n in the photographed xylem area A;  $\pi$  is pi;  $\rho$  and  $\eta$  are the density of water (996.7867 kg m<sup>-3</sup>) and water dynamic viscosity (8.9 × 10<sup>-4</sup> Pa s) at 26°C, respectively.

### Dominance-weighted traits

We used the species relative dominance (percentage stem basal area of each species in each forest) to calculate the dominance-weighted mean (DWM) for each hydraulic trait, which we use as an estimate of the community-weighted mean (CWM; Garnier et al., 2004). The DWM was calculated from a subsample of the species in each community once, as to achieve 50% of the hyperdiverse LSF dominance, it would require sampling at least 53 species. Our rationale relies on the fact that the DWM from a subsample of species in the community is valid as long as: (1) no single species and trait value exerts stronger influence over the CWM value; or (2) sample weight and sample value are independent, and the estimated weighted mean of a subsample of the data should approximate the true weighted mean (see Methods S1).

For both LSF and HSF we did not detect any relationship between the trait value and the species dominance, and the most dominant species were not outliers. Furthermore, to evaluate whether our results have biases due to the low coverage of basal area of the LSF, we carried out additional analyses to demonstrate that there was no change in the estimates when a larger data sample is considered. Since the contribution to the basal area is homogeneously distributed across many species and the traits are assumed to vary randomly, this enables us to assume the DWM as a good estimator of the CWM and scale results to the whole community. Additionally, we used the biogeographic dry-affiliation index as a trait of the genera in each site (Esquivel-Muelbert *et al.*, 2017, 2018; Methods S2) to evaluate the community

functional composition, that is, the dry affiliation of the whole community at each site.

### Microclimatic and soil data

We measured meteorological conditions at both eddy flux tower sites (1999 to 2016; update from Restrepo-Coupe *et al.*, 2016; details in Methods S3). For each location we used the cumulative monthly water deficit (CMWD; mm) as a measure of soil water deficit, calculated as in Aragão *et al.* (2007), except that we used a positive sign to denote convention for the deficit. CMWD was calculated for each month as the cumulative excess of evapotranspiration less precipitation, starting in the wet season of 1999 for LSF, and 2002 for the HSF: ()

$$CMWD_{m} = CMWD_{m-1} + ET_{m} - P_{m}$$

where ET<sub>m</sub> is monthly evapotranspiration (mm),  $P_{\rm m}$  is monthly precipitation (mm) and CMWD<sub>m</sub> is the cumulative water deficit for month m (mm) and CMWD<sub>m-1</sub> is that for the previous month. CMWD<sub>m</sub> was initialized at zero for the first month and was reset to zero whenever it became negative (i.e. there was a water surplus and not a deficit). The annual mean CMWD was  $43.6 \pm 47.3$  for the LSF, and  $109.1 \pm 49.4$  for the HSF, while the mean annual peak of CMWD was  $154.8 \pm 118.6$  mm for LSF, and  $333.1 \pm 110.8$  mm for the HSF (Fig. 1).

To verify that the estimated CMWD was a good proxy for the more physiologically relevant soil moisture deficit, we assessed the correlation of CMWD with monthly averaged soil volumetric water content (SWC) measurements (cm<sup>3</sup> cm<sup>-3</sup>) available at each site. The SWC was measured hourly from October 2015 to August 2016 at the LSF (depths of 0.8, 1.6, 2.4. m; L. Borma et al., unpublished data) and from August 2008 to March 2017 (with a 4-yr gap from 2012 to 2015) at the HSF (depths of 0.1, 1.0, 2.0 m; B. Christoffersen et al., unpublished data). We obtained soil water retention curves for LSF from L. Borma et al. (unpublished). Using the time series that overlaps between the two sites (2015 and 2016), the monthly CMWD explained 46% ( $F_{(1,9)} = 7.57$ ; P = 0.02 for LSF) and 65% ( $F_{(1,52)} = 95.49$ ; P < 0.001 for HSF) of the variation in the soil water content (0 to 2.0-2.4 m soil depth) (Fig. S2), confirming that CMWD could be used as a suitable proxy for soil water deficit.

### Canopy conductance

To obtain the ecosystem canopy conductance ( $G_S$ ; mm s<sup>-1</sup>) we used eddy covariance data from both sites (LBA data from 2002 to 2016, see Methods S3). We calculated  $G_S$  through the inversion of the Penman–Monteith (PM) equation (Methods S4). We restricted estimates of  $G_S$  to times when the canopy was dry (all data up to 12 h after precipitation were removed), so we could justifiably assume that most of the flux was due to transpiration. Eddy covariance, microclimatic and soil data are available at LBA

data repository (LBA DIS; see https://daac.ornl.gov/cgi-bin/data set\_lister.pl?p=11).

### Data analysis

To address our first hypothesis, whether traits from LSF species had less drought-resistant traits than HSF species, we used a one-tailed statistical Welch's *t*-test, and to evaluate the differences in dominance-weighted means we used a Monte Carlo approach with the difference in weighted mean as the test statistic, randomizing the site and repeating 10 000 times.

To evaluate our second hypothesis, whether the dry season leaf water potential ( $\Psi_{min}$ ) of the species was affected by the 2015-ENSO in relation to a non-ENSO year and whether the effect differed between sites, we used a general mixed model with species as random factor affecting intercept to account for the same species being measured in the ENSO and non-ENSO year in each site. This has a similar effect of pairing the species in a paired *t*-test. Additionally, to better understand ENSO effects, we evaluated whether  $\Psi_{min}$  variation could also be accounted by the atmospheric and soil water deficits (monthly maximum VPD and monthly CMWD) when the  $\Psi_{min}$  was measured. To evaluate if the species response to ENSO was modulated by hydraulic traits, we tested whether the difference in species  $\Psi_{min}$  from ENSO to non-ENSO year ( $\Delta\Psi$ ) was related to hydraulic traits using general fixed effects model.

For the third hypothesis, we evaluated whether effects of VPD and CMWD, measures of atmospheric and soil water stress, on G<sub>s</sub> differed between HSF and LSF. As periods of soil drought usually occur with atmospheric drought, we had to first remove the correlation between VPD and CMWD. For this we modelled VPD ~ CMWD and site to obtain a VPD independent from the CMWD measure (VPD<sub>r</sub> for VPD residuals). In the same way, we modelled CMWD ~ VPD and site to obtain a CMWD independent from VPD (CMWD<sub>r</sub>). With independent VPD and CMWD measures, we tested whether  $G_s$  had a fixed VPD<sub>r</sub> and CMWD<sub>r</sub> effect and whether site (HSF and LSF) had an additive or interactive effect on  $G_s$ . For the above analysis and for obtaining CMWD<sub>r</sub> and VPD<sub>r</sub>, we used general mixed effect models, with month of the year as random factor affecting slope, to control for temporal autocorrelation of variables. The same analyses were performed to evapotranspiration (ET). Finally, to evaluate whether the ecosystem-level water use (G<sub>s</sub>) was modulated by hydraulic traits, we analysed if dominance-weighted P<sub>50</sub> and hydraulic safety margin affected  $G_s$ .

Part of the difficulty in analysing atmospheric and soil drought effects is that both are usually correlated (i.e. rainless periods usually have drier atmosphere). To remove this correlation from our dataset, we used only data with CMWD higher than 0, and observations from July to December of 2015. This approach was justified as our goal is to evaluate drought response of  $G_s$ , and the data from January to June is usually rainy (precipitation > 100 mm month<sup>-1</sup>). Moreover, LSF had almost no data with CMWD > 0 mm in this wet period, and it would only carry information about  $G_s$  response to VPD in wet conditions. For all statistical analyses, data processing and curve fitting, we used R

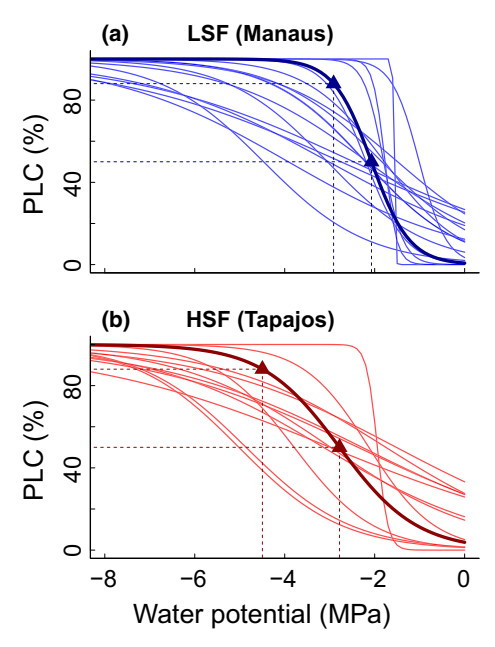


**Fig. 2** Hydraulic vulnerability curves for different species at (a) LSF (low seasonal forest) and (b) HSF (high seasonal forest). The thicker lines denote the dominance-weighted vulnerability curve for each forest (blue for LSF and red for HSF).

(R Core Team, 2018, v.3.5), and further information about the analysis functions and packages can be found in the Supporting Information Methods S5.

### **Results**

### Hydraulic trait differences between the two forests

The LSF had less embolism-resistant hydraulic vulnerability curves than HSF due to higher  $P_{88}$  (-4.08  $\pm$  1.83 MPa vs  $-5.33 \pm 1.49$  MPa, P = 0.027; Fig. 2), and a marginally significant difference in  $P_{50}$  between the two forests ( $-2.34 \pm 0.89$  MPa and  $-2.90 \pm 1.15$  MPa, respectively, P = 0.085; Figs 2, 3a; see Tables S1 and S2 for results summary). Different P<sub>88</sub>, even if the P<sub>50</sub> was similar, is only possible if HSF has a shallower slope than LSF species hydraulic vulnerability curves, consistent with our observations of a marginally significant difference in slopes (Fig. 2; slope difference P = 0.07; Table S2). Corroborating these results, the dry-affiliation index (represented by the probability of recording a higher dry-affiliated precipitation centre of gravity value than that observed by chance) revealed differences in the HSF and LSF community functional composition (details in Methods S2). We found a dominance of dry-affiliated taxa for HSF compared to LSF  $(0.73 \pm 0.4 \text{ for HSF and } 0.86 \pm 0.3 \text{ for LSF}; t = 4.8,$ df = 339.9, P < 0.001) (Fig. 4).

The minimum water potential in the non-ENSO year  $(\Psi_{\text{nonENSO}})$  was higher (P < 0.01) in the LSF  $(-1.09 \pm 0.43 \text{ MPa})$  than in HSF  $(-1.88 \pm 0.58 \text{ MPa})$ , however the hydraulic safety margins (i.e. non-ENSO HSM<sub>P50</sub> and HSM<sub>P88</sub>) did not differ between the two forests (P = 0.38 and P = 0.23) (Fig. 3c–e; Table S2). The xylem anatomy of the HSF and LSF species also showed significant differences for all

inspected traits: vessel density, vessel area, potential specific hydraulic conductance and hydraulic diameter (Fig. 3f–i; Table S2). Xylem vessel area was higher at the LSF site than at the HSF site (P=0.03), and so were the hydraulic diameter (P=0.04) and the potential specific conductance (P=0.04; Fig. 3, Table S2), while the vessel density was 71% higher at HSF (P=0.01; Fig. 3f; Table S2).

The analysis comparing the dominance-weighted mean of LSF and HSF showed similar patterns, with  $P_{88}$  of HSF forest being lower than LSF, and  $P_{50}$  and slope marginally different (see Table S2). However, this analysis did not detect differences in anatomical traits, possible because of the lower statistical power of the test and the high value of the 95% confidence intervals of the mean for those traits.

# Species- and community-level responses to the 2015-ENSO-induced drought

The 2015-ENSO climatic effects were observed in both forests, as the CMWD reached values higher than historical means of the driest months recorded since 1998 (Fig. 1). The 2015-ENSO-induced CMWD was largest in the HSF, but absolute and relative changes from the 1998–2014 average of annual maximum CMWD were higher in LSF, with an increase of 306.4 mm (197-%; 154.8–461.2 mm) vs 155 mm (46%; 333.1–488.1 mm) in HSF. The  $\Psi_{\rm nonENSO}$  and  $\Psi_{\rm ENSO}$  measurements at the LSF site were performed during a CMWD of 67.4 mm, and 356.1 mm, respectively; whereas in the HSF,  $\Psi_{\rm nonENSO}$  and  $\Psi_{\rm ENSO}$  were measured when the CMWD reached 303.2 mm and 422.3 mm, respectively (Figs 1, 5a), confirming the different CMWD conditions when the  $\Psi_{\rm min}$  was measured in both forests.

At both LSF and HSF sites,  $\Psi_{\rm min}$  was significantly reduced during the ENSO period (P<0.001; see Table S3 for statistical summaries), although the effect of ENSO on  $\Psi_{\rm min}$  was not very large (0.6 and 0.5 MPa drop for LSF and HSF, respectively). Site had an additive effect on  $\Psi_{\rm min}$  (P=0.006), with the HSF  $\Psi_{\rm min}$  being on average -0.72 MPa lower than LSF (Fig. 5a), but there was no interaction between site and ENSO (P=0.12), indicating the 2015-ENSO effect on  $\Psi_{\rm min}$  was similar in both areas. The model explained 68% of  $\Psi_{\rm min}$  variability, where ENSO and site explained 32% (conditional and marginal  $R^2$ , respectively).

At the species level, responses to the 2015-ENSO event were heterogeneous (Fig. 5b,c). At the LSF site,  $\Psi_{\min}$  declined in almost all species during ENSO, while at HSF the responses were more diverse, with a majority of species (*Miconia* sp., *C. albescens*, *E. uchi* and *R. pubiflora*, *M. itauba*) showing a steep drop in  $\Psi_{\min}$ , while a minority (four of nine) showed no detectable change (the slight increases seen in Fig 5 are in the range of the measurement error).

Monthly maximum VPD was related to  $\Psi_{\rm min}$  (P<0.001; Fig. 5c, Table S3) but only with a significant site interactive (P=0.008) and additive (P=0.001) effect on VPD. CMWD was related to  $\Psi_{\rm min}$  (P<0.001; Fig. 4b; Table S3) but site had no interactive or additive effect on  $\Psi_{\rm min}$  (P=0.31 and P=0.11). The CMWD and VPD of this dataset were related (r=0.56) as the month with higher VPD also had higher CMWD, which

precludes us from inferring whether the VPD or CMWD effect is dominating the  $\Psi_{min}$  variability. However, VPD requiring additional explanation of site to explain  $\Psi_{min}$  suggests that CMWD contains additional information not contained in VPD, possibly the correlation with site, which absorbed the site effect on  $\Psi_{min}$ , making CMWD the only significant effect in the model. This effect can be seen in Fig. 5(b,c).

The leaf water potential change, comparing non-ENSO to 2015-ENSO ( $\Delta\Psi$ ), was related to embolism resistance for both P<sub>50</sub> and P<sub>88</sub> (P=0.017;  $r^2$ =0.21 and P=0.019;  $r^2$ =0.21, respectively; Fig. 6). Species with higher embolism resistance had higher changes in  $\Delta\Psi$ . Site effects on P<sub>50</sub> and P<sub>88</sub> were not significant for additive effect (P=0.77 and P=0.32) or interaction effect (P=0.15 and P=0.13), indicating  $\Delta\Psi$  is similarly modulated by embolism resistance in both sites. Anatomical traits were not related to  $\Delta\Psi$  (P>0.20 for all anatomical traits). P<sub>50</sub> and P<sub>88</sub> had the same explanatory power of  $\Delta\Psi$  ( $r^2$ =0.21), likely due to both being strongly correlated (r=0.74).

## Ecosystem-level functional responses to drought

Both CMWD and VPD from July to December were highly correlated (r=0.41), particularly for HSF (r=0.53). This correlation was removed using the residuals of one variable modelled with the other as predictor and site as additive factor (Table S4). The residuals of VPD (VPD<sub>r</sub>) did not carry any more signal of CMWD for both sites (r<0.01), and the residuals of CMWD (CMWD<sub>r</sub>) did not carry any VPD signal (r=-0.07).

Canopy conductance  $(G_s)$  was significantly affected by VPD<sub>r</sub>  $(P < 0.001; R^2 = 0.40)$ , with no additive or interactive site effect, while CMWD<sub>r</sub> was unrelated to  $G_s$  (P = 0.10; Fig. S3; Table S4). Given the lack of evidence for a VPD-independent signal of CMWD on  $G_s$ , we remodelled  $G_s$  as a function of VPD (Fig. 7). We found each unit of VPD caused a decreased in  $G_s$  of 5.1 mm s<sup>-1</sup> (P < 0.001) and VPD explained 40% of  $G_s$  variability. Site had no significant additive or interactive influence on  $G_s$  (P = 0.91) and (P = 0.08), indicating HSF and LSF respond

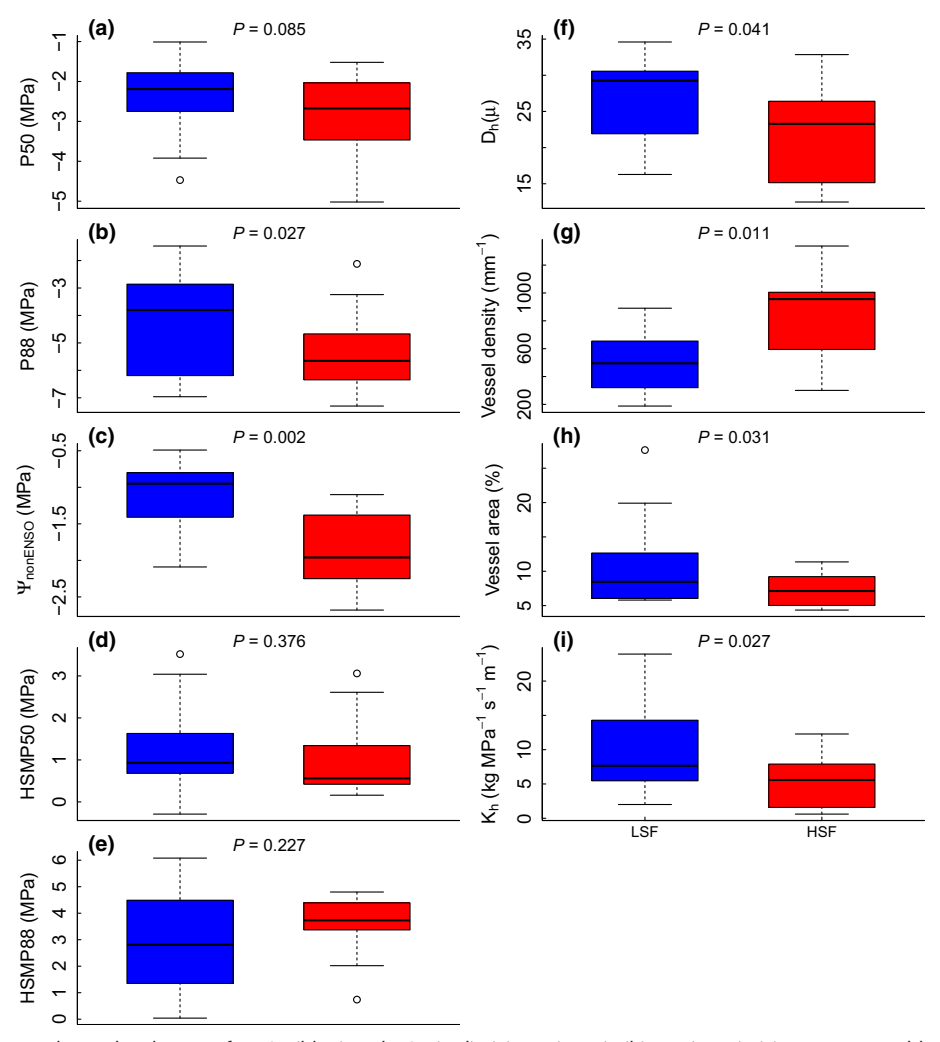


Fig. 3 Hydraulic and anatomical trait distributions for LSF (blue) and HSF (red): (a)  $P_{50}$  (MPa); (b)  $P_{88}$  (MPa); (c) minimum midday (12:00–14:30 h) water potential for the non-ENSO year (MPa); (d)  $P_{50}$  hydraulic safety margin for the non-ENSO year (MPa); (e)  $P_{88}$  hydraulic safety margin for the non-ENSO year (MPa); (f)  $D_v$  – Hydraulic diameter (mm), (g) Vessel density (vessels mm<sup>-2</sup>); (h) Vessel area (% vessel area per xylem area); and (i) Potential specific conductance ( $K_h$ ; kg MPa<sup>-1</sup> s<sup>-1</sup> m<sup>-1</sup>). Whiskers are either maximum/minimum value or, when outliers are present, 1.5 interquartile range above/below the quartiles 2 and 3.

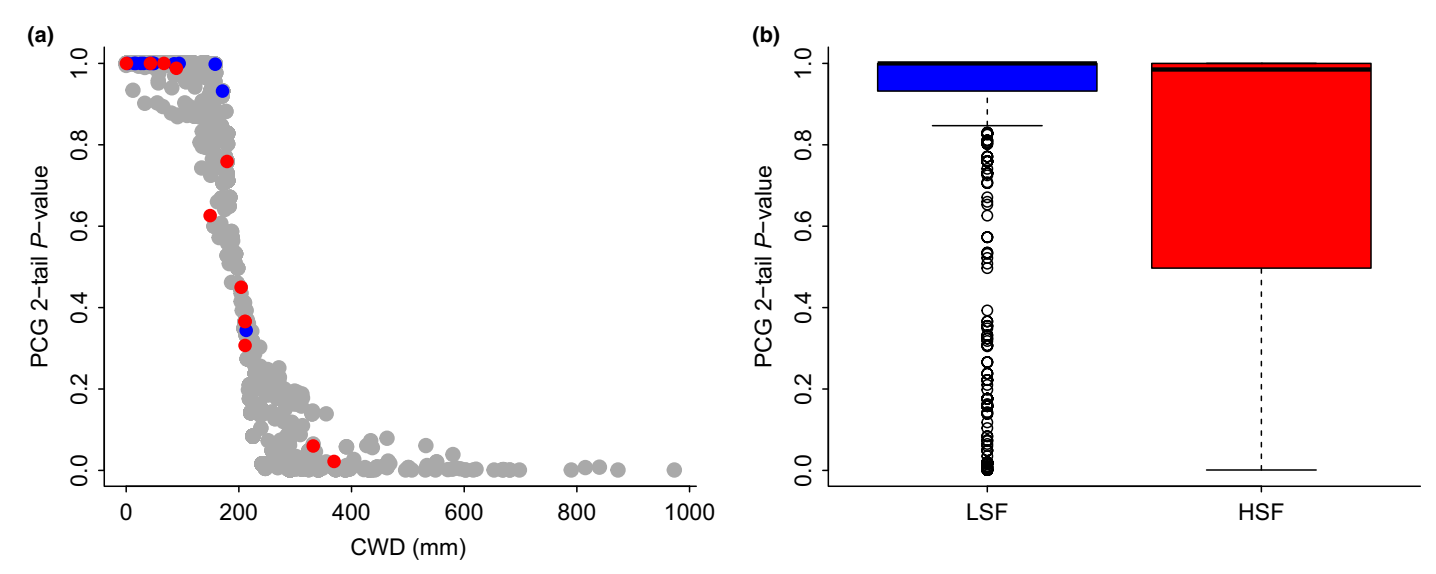


Fig. 4 (a) The probability of recording a higher dry-affiliated precipitation centre of gravity (PCG) value than observed by chance (PCG 2-tail P-value) for a range of genera in Amazonian sites varying with the Cumulative Water Deficit for the same sites obtained by Esquivel-Muelbert et~al. (2017). Each point represents a different genus in the Amazon (grey points), where blue and red points represent the studied genera for LSF and HSF, respectively. (b) The PCG 2-tail P-value obtained from the database available at Esquivel-Muelbert et~al. (2017) for the all the genera recorded at LSF (blue) and HSF (red). The higher the genus PCG 2-tail P-value, the lower its dry affiliation index. We can see the lower dry affiliation of LSF genera (higher PCG 2-tail P-value, P0.001) when compared with the HSF genera. Whiskers in (b) are minimum value or, when outliers are present, 1.5 interquartile range below the quartile 2.

equally to VPD. Evapotranspiration (ET) was not affected by VPD<sub>r</sub> neither was CMWD<sub>r</sub> (P=0.32 and P=0.29), although site had a significant effect on ET (P<0.001) (Table S5; Fig. S4).

The differences in ecosystem canopy conductance  $(G_s)$  values between the two forests correlated with the variation observed in community  $\Psi_{\min}$ , as represented by the dominance-weighted trait (Fig. 8). For the same  $G_s$  value, the HSF had more negative community  $\Psi_{\min}$  than LSF, and the  $G_S$  seems to respond linearly to HSM<sub>P50</sub>, which explained 95% of  $G_s$  variability, when the two sites were considered together (P= 0.02) (Fig. 8b).

## **Discussion**

We evaluated plant responses at the species, community and ecosystem levels during typical years and one of the most severe drought events (El-Niño event in 2015) (Jiménez-Muñoz *et al.*, 2016) ever recorded in Amazonia. We report species-level hydraulic traits that contributed to the observed differences in forest drought responses. Our findings highlight the role of rainfall seasonality and interannual variability in precipitation as important filters selecting different hydraulic traits, strategies and taxa across rainforest sites, and complement analyses based on MAP differences alone (Choat *et al.*, 2012; Ciemer *et al.*, 2019). The dominant species at the high seasonality forest in the eastern Amazon (HSF) are more drought-affiliated and exhibit hydraulic traits with higher embolism resistance (i.e. lower P<sub>88</sub>), as compared to the low seasonal forest in the central Amazon (LSF).

Despite this difference in the hydraulic system of the plants, both forests maintained the same sensitivity of canopy conductance ( $G_s$ ) to atmospheric drought. Our data suggest this is possible because of the higher embolism resistance in HSF.

Interestingly, the two forests had similar responses to the 2015-ENSO when we consider their change in water potential, and at both forests we showed species embolism resistance modulated the species-level response to ENSO. Importantly, despite the limitations of our sampling design, we were able to show that species-level hydraulic traits have the potential of being scaled up to community-level properties, which in turn could help in explaining ecosystem-level water fluxes and drought response (Fig. 8).

# Differences in drought resistance traits between low and high seasonality forests

Our results indicate that precipitation regime is an important filter in selecting contrasting embolism vulnerabilities. The drier condition and the marked seasonality and interannual rainfall variability in eastern Amazon make the HSF an environment with more pronounced water limitation, which in turn, has shaped the dominance of traits related to embolism resistance that allowed species to operate at more negative  $\Psi$  during water-limiting conditions. Consistent with these findings, our results indicate a higher proportion of dry-affiliated taxa at the HSF when compared with the LSF (Fig. 4) (Esquivel-Muelbert *et al.*, 2017), and the dominance of drought-resistant taxa in the HSF also suggests that climate-driven community assembly may be the mechanism underlying the higher resilience to climatic disturbances observed for forests under higher rainfall variability regimes in the Amazon (Ciemer *et al.*, 2019).

The differences between  $P_{88}$  and  $P_{50}$  show that xylem embolism resistance (represented by the vulnerability curve) can be affected not only by shifting the curves towards a certain  $P_{50}$ , but also by modifying their shape (i.e. the slope and the

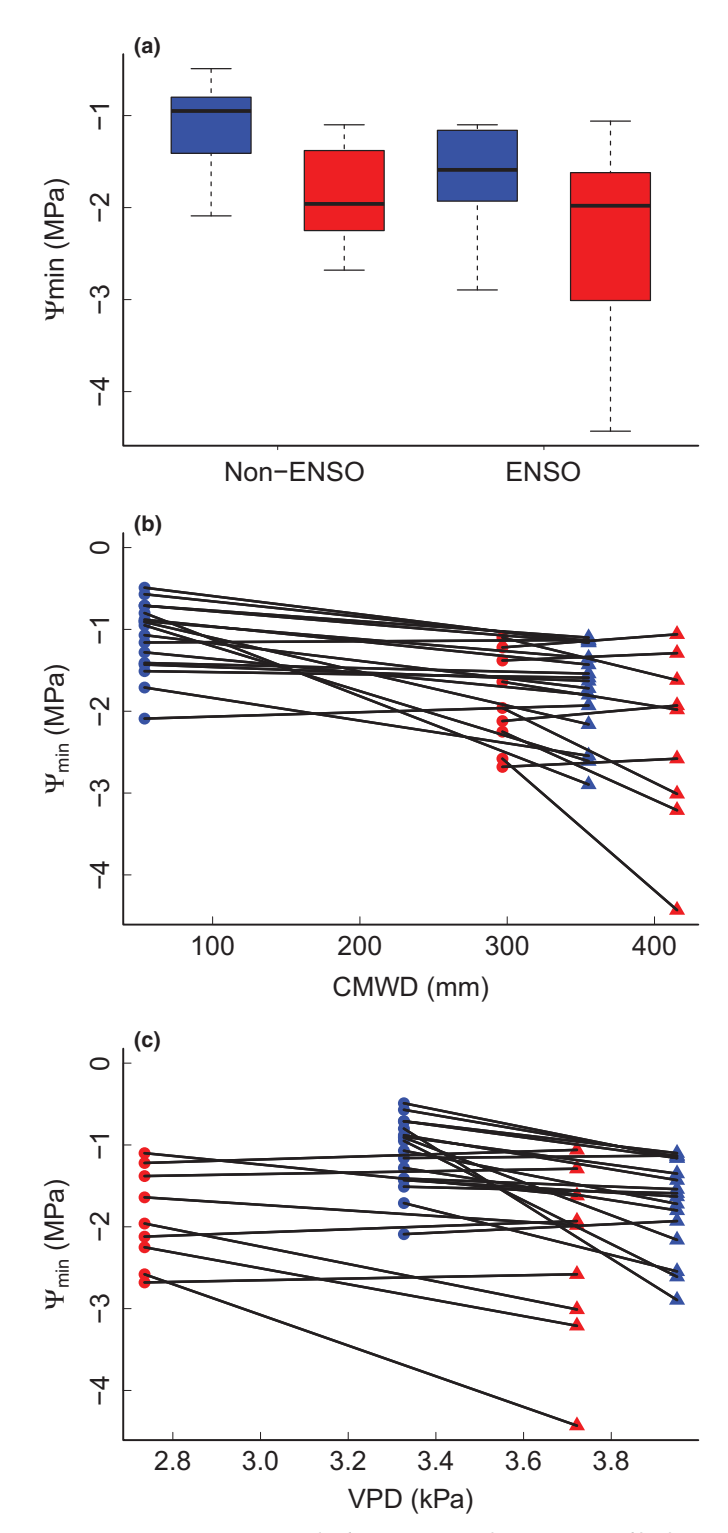


Fig. 5 (a) Dry season minimum leaf water potential ( $\Psi_{min}$ ; MPa) of high seasonality forest (HSF; Tapajos) and the low seasonality forest (LSF; Manaus) species during non-ENSO year (blue) and the 2015-ENSO year (red). Change in minimum leaf water potential ( $\Psi_{min}$ ; MPa) from non-ENSO (circles) to the 2015-ENSO year (triangles) in the low seasonality forest (LSF, Manaus; blue) and the high seasonality forest (HSF, Tapajos, red) as a function of monthly CMWD, and (b) maximum monthly vapour pressure deficit (VPD); (c) Each pair of points (circle and triangle) represents a different species.

difference between P<sub>50</sub> and P<sub>88</sub>) (Fig. 2). We observed a lower P<sub>88</sub> in the HSF, which could be an evolutionary adjustment allowing these species to maintain xylem conductivity in highly seasonal environments where some embolism may be unavoidable, mainly for shallow-rooted species in HSF (Brum *et al.*, 2018). Thus, we emphasize the importance of xylem embolism resistance (represented by the vulnerability curves) as one of key functional traits relevant for explaining the patterns of plant distribution in biodiverse tropical ecosystems, as proposed for other environments (Pockman & Sperry, 2000; Brodribb, 2017; Cosme *et al.*, 2017; Trueba *et al.*, 2017; Oliveira *et al.*, 2019).

# Complex leaf water potential response to the 2015-ENSO-induced drought

During the 2015-ENSO, the Amazon Basin-wide average temperature reached a record high (annual monthly maximum was 2.5°C higher than the climatological mean) for the last century, exacerbating the effect of the 2015-ENSO drought (Jiménez-Muñoz *et al.*, 2016; Panisset *et al.*, 2018). The warmer conditions increased the evaporative demand (VPD) at both sites, affecting species hydraulic functioning. Our results showed a site-specific condition affecting  $\Psi_{\min}$  (Fig. 5), with the CMWD likely incor-

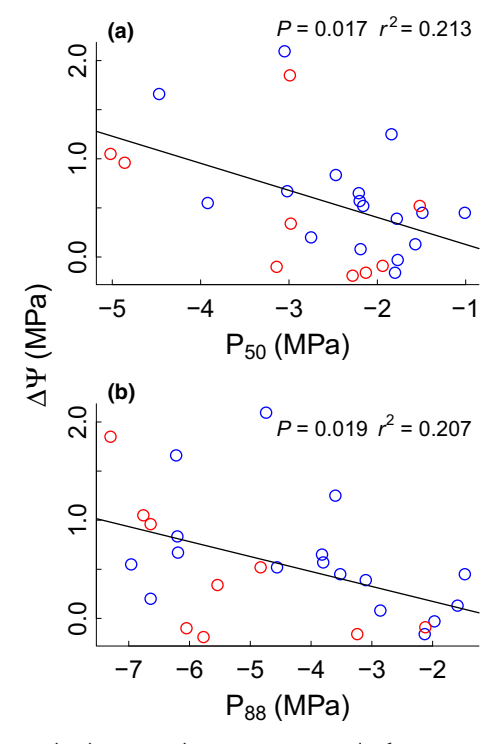


Fig. 6 Relationship between change in minimum leaf water potential from non-ENSO year to 2015-ENSO year ( $\Delta\Psi$ ; MPa) and embolism resistance for the low seasonality forest (LSF, Manaus, blue) and the high seasonality forest (HSF, Tapajos, red). Relationship between  $\Delta\Psi$  and (a) P<sub>50</sub> and (b) P<sub>88</sub>. The solid lines represent the best linear fit. Whiskers in (a) are either maximum/minimum value or, when outliers are present, 1.5 interquartile range above/below the quartiles 2 and 3.

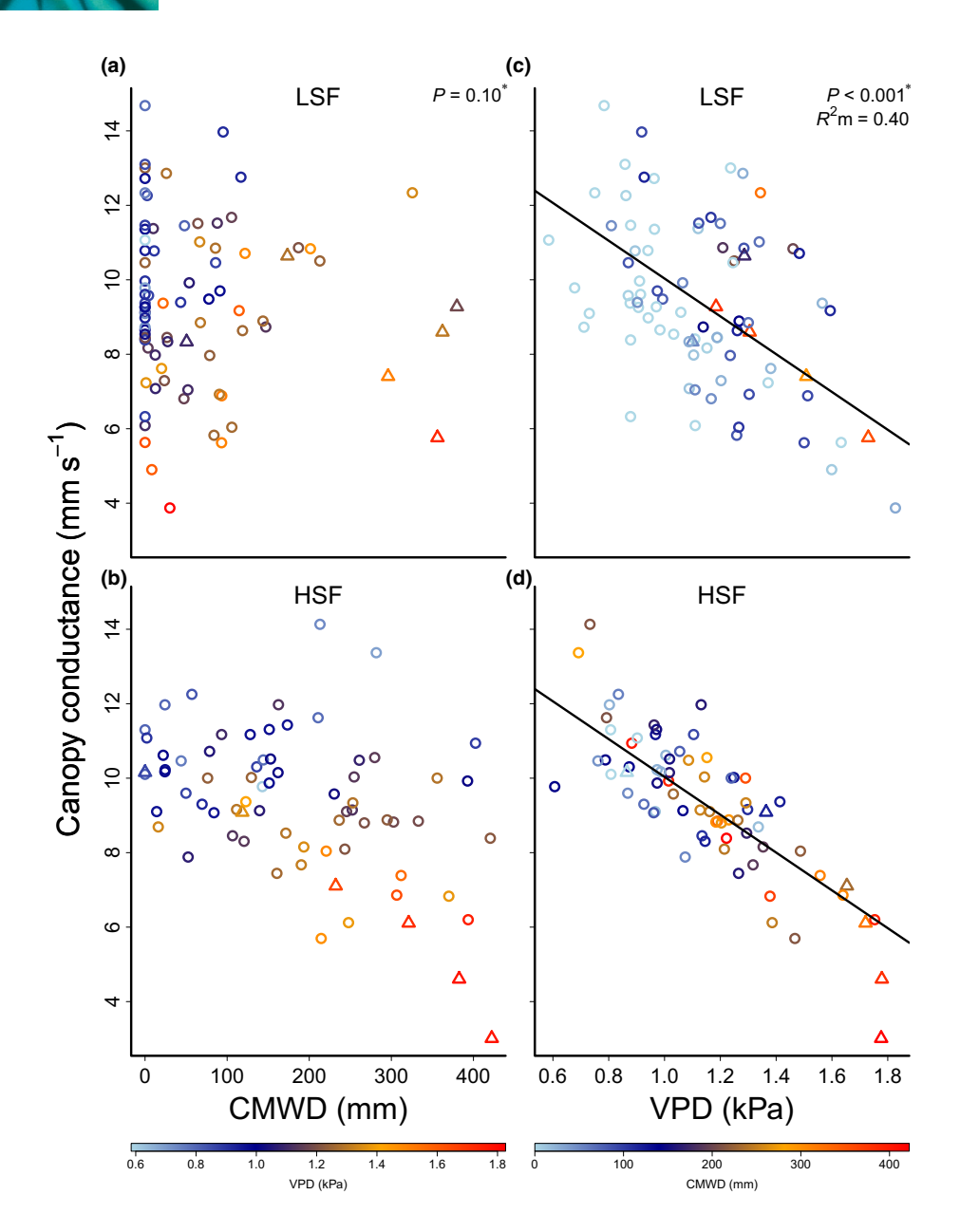


Fig. 7 Relationship between July to December monthly mean canopy conductance ( $G_S$ ) and cumulative water deficit (CMWD) in (a) low seasonality forest (LSF, Manaus) and (b) high seasonality forest (HSF, Tapajos), and between canopy conductance (Gs) and monthly mean vapour pressure deficit (VPD) for (c) LSF and (d) HSF. The colour of the data points is proportional to the VPD value in plots (a) and (b) and to the CMWD values in plots (c) and (d), according to the colour charts below the panels. Note that high CMWD data points are redder, indicating they also have high VPD showing the correlation between VPD and CMWD. The P-values\* are for the relationship between  $G_s$  and VPD<sub>r</sub> and CMWD<sub>r</sub>, which are the same variables after removing the correlation between VPD and CMWD using residuals (see the Data analysis subsection and the Results). Note both sites were modelled together and the P-value in panel (a) also applies to (b), and P and  $R^2$  values in (c) also apply to (d). Triangle points are data from 2015-ENSO. Circle points are monthly data from 1999 to 2016, excluding the 2015-ENSO period. Another version of this figure presenting the  $G_s$ relationship to VPD<sub>r</sub> and CMWD<sub>r</sub> is presented in Supporting Information Fig. S3.

porating both the atmospheric signal (VPD) and the soil signal (CMWD) in plant water potential.

This difficulty in separating soil and atmospheric water stress, as both usually occur together, is furthermore complicated by the non-linear effect of soil water content (represented in our study sites by the CMWD) on soil water potential (van Genuchten, 1980), which means it is necessary to have substantial decrease in CMWD for the soil water potential to increase to levels that induce embolism; and once this threshold is reached a small change in CMWD implies a large change in soil water potential. This threshold has an important consequence for vegetation, as it represents the point when plants start experiencing a strong soil drought signal, which depends on: (1) soil type and soil depth, (2) tree rooting depth, and (3) spatial variability, all factors that can imply landscape niches with different degrees of vulnerability. So, depending on the locations and species, the CMWD can

have different meanings, and should be used with caution as universal index of drought stress for vegetation (Esquivel-Muelbert *et al.*, 2017). For example, the higher drop in Ψ observed for some species at the HSF could indicate the placement of their roots in shallow soils and less stomatal regulation, while deeprooted species probably avoid extreme intensity of droughts (e.g. Nepstad *et al.*, 1994; Oliveira *et al.*, 2005; Ivanov *et al.*, 2012; Brum *et al.*, 2018).

Although we observed a strong climatological drought, we cannot predict its consequences for long-term functioning of trees, as it does not immediately translate to ecohydrological drought (Nepstad *et al.*, 2007; Da Costa *et al.*, 2010) and some species were still operating within some hydraulic safety margin. We found the drought was enough to cause a modest average drop in leaf  $\Psi$  (with  $\Psi$  stabilization), probably indicating species stomatal control, with the major effect at gas exchange level, as observed

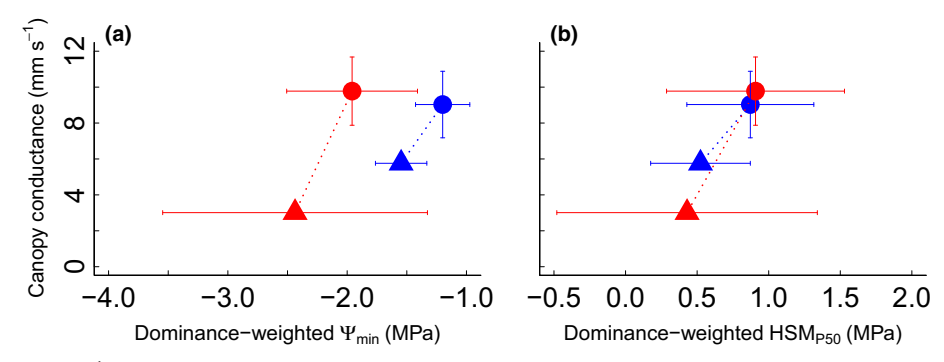


Fig. 8 Canopy conductance (mm s $^{-1}$ ) in non-ENSO (circles) and ENSO (triangles) years and for LSF (blue) and HSF (red) vs: (a) the dominance-weighted minimum leaf water potential ( $\Psi_{min}$ ; MPa), and (b)  $P_{50}$  hydraulic safety margin (HSM $_{P50}$ ; MPa). The horizontal bars represent the confidence interval (ci) for the dominance-weighted mean of  $\Psi_{min}$  and HSM. The vertical bars represent the SD, across typical years, of canopy conductance in August and December for LSF and HSF, respectively. We considered as typical (non-ENSO) years the period from 1999 to 2016, excluding data from 2015-ENSO. As ENSO year, we considered October and December of 2015 for LSF and HSF, respectively, and hence we had no monthly SD.

with the decrease in  $G_s$ , which is likely maintaining ET constant despite changing VPD, as predicted by stomatal optimization models (Sperry & Love, 2015; Eller *et al.*, 2018). We also show that xylem embolism resistance explained part of the response in leaf  $\Psi$  during the 2015-ENSO (Fig. 6), which means species with higher resistance to xylem embolism could withstand lower water potentials and maintain gas exchange under drier conditions. Thus, to obtain a more comprehensive understanding on the diversity of plant water potential responses, studies should consider traits that influence plant water supply, demand and storage, some of which are very challenging to measure in the field.

# Canopy conductance changes as an ecosystem-level response

It is notable that, despite the HSF and LSF operating at different  $\Psi_{\rm min},$  both had the same canopy-level response to VPD (Fig. 7). This difference between water supply function responses with no difference in the canopy-level water control function responses is likely possible only because the HSF has a more embolism-resistant water transport system. This is theoretically expected, as the embolism resistance sets the water potentials under which plants can operate (Sperry & Love, 2015) and, consequently, modulate the atmospheric and soil climatic envelope they can tolerate.

In fact, we show here the  $\Psi_{min}$  and HSM are traits mechanistically involved in species physiological responses under different conditions of water availability (Fig. 8). Moreover, the result that both communities operate under the same safety margin, in ENSO and non-ENSO, suggests they can retain their gas exchange rates even under extreme drier conditions than the usual dry season, which probably directly influences forest productivity. This highlights the role of xylem embolism resistance traits in determining plant functioning and vegetation drought response (Anderegg *et al.*, 2016, 2018). Actually, including embolism resistance in plant models has improved the prediction of ecosystem transpiration drought responses in the Amazon forest of Caxiuanã (Eller *et al.*, 2018), and such models also predict lower sensitivity to drought than previous models, a result supported by our data.

Despite changes in the CMWD we did not detect its signal in canopy-level response. In LSF, the effect of 2015-ENSO was only substantial in the superficial soil layers (c. 80 cm depth), suggesting that a higher CMWD (than that caused by the 2015-ENSO) is necessary to affect deeper soils and change the soil water content in a way that would induce notable changes in canopy conductance. On the other hand, in the HSF, the large variability in soil water content (at least to a depth of 2 m; Fig. S2) did not affect Gs either, emphasizing the importance of more drought-resistant traits and/or deeper roots to modulate canopy water use. This suggests possibly extreme dry years, and not average years, contribute to filter plant communities, where trees have adapted their water transport system to drier than normal conditions, which they will likely experience during their lifespan (Grant et al., 2017). Moreover, as in HSF trees are currently operating at lower soil water availability, we believe that an additional increase in CMWD may provoke extreme changes in soil water potential (Hutyra et al., 2005) and consequently in forest functioning. Additional studies will need to consider interactions between rooting depth and soil moisture dynamics to gain insights into the behaviour of forest canopy conductance.

#### Conclusion

We report significant differences in hydraulic traits between two Amazon forests: low (LSF) and high (HSF) seasonal forest. Our results demonstrate that the seasonal and interannual variability in water stress is a key factor driving hydraulic functional differences across tropical forest sites. Interestingly, despite differences in water transport operation and traits, this difference was not translated into different atmospheric drought responses, suggesting the more drought-resistant hydraulic traits in HSF compensated for the drier soils, equalizing their safety margin and allowing them to maintain similar canopy-level responses to a drier atmosphere in both forests.

Our study shows the importance of embolism resistance in explaining interspecific variability in drought responses of the two different communities of species that have contrasting seasonality of moisture availability, thereby linking relevant traits to species distribution, community assembly and ecosystem functioning. Further studies should address how spatial and temporal climatic variability at broader scales in the Amazon region filter a set of hydraulic traits that affect forest functioning, which will permit better-informed predictions of vegetation response to climate change.

# **Acknowledgements**

We acknowledge funding from Brazil-USA Collaborative Research GoAmazon (DE-FOA-0000919, FAPESP-2013/50531-2, FAPESP-2013/50533-5), Microsoft/FAPESP-2011/52072-0, US DOE nos. DE-SC0008383 and DE-SC0011078. NSF#1622721 supported NRC and K67 eddy-flux data. We thank CAPES for support of the scholarships of FdVB, PRB, MB, and other co-authors, and CNPq for RSO's productivity scholarship. VI acknowledges support from Google Inc. towards the project 'Evapotranspiration of the Green Ocean Amazon'. We thank the Newton International Fellowship (NF170370) who recently funded PRLB. We thank the Large-Scale Biosphere–Atmosphere (LBA) Program and Empresa Brasileira de Pesquisa Agropecuária (EMBRAPA, Santarem) for technical support. We thank Mr Kleber Campos and Dr Kenia Wiedemann for their support.

#### **Author contributions**

FdVB, PRLB, MB and RSO conceived the research ideas, developed the project and wrote the manuscript. FVB, PRLB and MB collected, processed and analysed the data. N-RC and SRS, with support from PG, derived the ecosystem analysis, principally metrics of whole forest water cycling (canopy conductance and cumulative water deficit) from eddy covariance data, after applying consistent processing and QA/QC protocols at both sites. LSB and BOC collected and processed soil data. DP, LP and GST collected and processed some tree hydraulic data. LFA, AJNL and VMCC collected, processed and analysed floristic data. LSML and ACA maintained instruments and acquired and processed raw eddy covariance data from the low-seasonality forest (K34), and SRS and NR-C played this role at the HSF (K67). LOECA, J-EL and VI and all authors revised the manuscript. FdVB, PRLB and MB contributed equally to this work.

### **ORCID**

Luciana F. Alves https://orcid.org/0000-0002-8944-1851 Fernanda de V. Barros https://orcid.org/0000-0003-3835-2020

Bradley O. Christoffersen https://orcid.org/0000-0002-4890-9999

Rafael S. Oliveira https://orcid.org/0000-0002-6392-2526 Luciano Pereira https://orcid.org/0000-0003-2225-2957 Grazielle S. Teodoro https://orcid.org/0000-0002-5528-8828

## References

- Anderegg WRL, Flint A, Huang C, Flint L, Berry JA, Davis FW, Sperry JS, Field CB. 2015. Tree mortality predicted from drought-induced vascular damage. *Nature Geoscience* 8: 367–371.
- Anderegg WR, Klein T, Bartlett M, Sack L, Pellegrini AF, Choat B, Jansen S. 2016. Meta-analysis reveals that hydraulic traits explain cross-species patterns of drought-induced tree mortality across the globe. *Proceedings of the National Academy of Sciences, USA* 113: 5024–5029.
- Anderegg WRL, Konings AG, Trugman AT, Yu K, Bowling DR, Gabbitas R, Karp DS, Pacala S, Sperry JS, Sulman BN et al. 2018. Hydraulic diversity of forests regulates ecosystem resilience during drought. Nature 561: 538–541.
- Aragão LEOC, Malhi Y, Roman-Cuesta RM, Saatchi S, Anderson LO, Shimabukuro YE. 2007. Spatial patterns and fire response of recent Amazonian droughts. *Geophysical Research Letters* 34: L07701.
- Araujo AC, Nobre AD, Kruijt B, Elbers JA, Dallarosa R, Stefani P, von Randow C, Manzi O, Manzi AO, Culf AD et al. 2002. Comparative measurements of carbon dioxide fluxes from two nearby towers in a central Amazonian rainforest: the Manaus LBA site. Journal of Geophysical Research 107: 8090.
- Brienen RJW, Phillips OL, Feldpausch TR, Gloor E, Baker TR, Lloyd J, Lopez-Gonzalez G, Monteagudo-Menzoza A, Malhi Y, Martinez RA *et al.* 2015. Long-term decline of the Amazon carbon sink. *Nature* 519: 344–348.
- Brodribb TJ. 2017. Progressing from "functional" to mechanistic traits. New Phytologist 215: 9–11.
- Brum M, Vadeboncoeur MA, Ivanov V, Asbjornsen H, Saleska S, Alves LF, Penha D, Dias JD, Aragão LEOC, Barros F et al. 2018. Hydrological niche segregation defines forest structure and drought tolerance strategies in a seasonal Amazon forest. *Journal of Ecology* 107: 318–333.
- Carneiro VMC. 2004. Composição florística e análise estrutural da floresta primária de terra firme na bacia do Rio Cuieras, Manaus AM. Masters Thesis, Universidade Federal do Amazonas, Manaus AM, Brazil.
- Choat B, Jansen S, Brodribb TJ, Cochard H, Delzon S, Bhaskar R, Bucci GS, Field TS, Gleason SM, Hacke UG et al. 2012. Global convergence in the vulnerability of forests to drought. Nature 491: 752–755.
- Ciemer C, Boers N, Hirota M, Kurths J, Muller-Hansen F, Oliveira RS, Winkelmann R. 2019. Higher resilience to climatic disturbances in tropical vegetation exposed to more variable rainfall. *Nature Geoscience* 12: 174–179.
- Collatz GJ, Ball JT, Grivet C, Berry JA. 1991. Physiological and environmental regulation of stomatal conductance, photosynthesis and transpiration: a model that includes a laminar boundary layer. Agricultural and Forest Meteorology 54: 107–136.
- Cosme LHM, Schietti J, Costa FRC, Oliveira RS. 2017. The importance of hydraulic architecture to the distribution patterns of trees in a central Amazonian forest. *New Phytologist* 215: 113–125.
- Cox PM, Betts RA, Collins M, Harris PP, Huntingford C, Jones CD. 2004. Amazonian forest dieback under climate-carbon cycle projections for the 21<sup>st</sup> century. *Theoretical and Applied Climatology* 78: 137–156.
- Cox PM, Pearson D, Booth BB, Friedlingstein P, Huntingford C, Jones CD, Luke CM. 2013. Sensitivity of tropical carbon to climate change constrained by carbon dioxide variability. *Nature* 494: 341–344.
- Da Costa CL, Galbraith D, Almeida S, Tanaka Portela BT, da Costa M, de Athaydes SJ, Braga AP, Gonçalves PHL, Oliveira AAR, Fisher R *et al.* 2010. Effect of seven years of experimental drought on the aboveground biomass storage of an eastern Amazonian rainforest. *New Phytologist* 187: 579–591.
- Davidson E, Lefebvre PA, Brando PM, Ray DM, Trumbore SE, Solorzano LA, Ferreira JN, Bustamante MMC, Nepstad DC. 2011. Carbon inputs and water uptake in deep soils of an eastern Amazon forest. Forest Science 57: 51–58.
- De Gonçalves LGG, Borak JS, Costa MH, Saleska SR, Baker I, Restrepo-Coupe N, Muza MN, Poulter B, Verbeeck H, Fisher JB et al. 2013. Overview of the large-scale biosphere–atmosphere experiment in Amazonia data model intercomparison project (LBA-DMIP). Agricultural and Forest Meteorology 182–183: 111–127.
- Eller CB, Rowland L, Oliveira RS, Bittencourt PRL, Barros FV, Friend AD, Mencuccini M, Sitch S, Cox P. 2018. Modelling tropical forest responses to drought and El Niño with a stomatal optimization model based on xylem

- hydraulics. Philosophical Transactions of the Royal Society of London. Series B: Biological Sciences 373: 20170315.
- Engelbrecht BMJ, Comita LS, Condit R, Kursar TA, Tyree MT, Turner BL, Hubbell SP. 2007. Drought sensitivity shapes species distribution patterns in tropical forests. *Nature* 447: 80–82.
- Engelbrecht BMJ, Kursar TA, Tyree MT. 2005. Drought effects on seedling survival in a tropical moist forest. *Trees* 19: 312–321.
- Esquivel-Muelbert A, Baker TR, Dexter KG, Lewis SL, Brienen RJW, Feldpausch TR, Loyd J, Monteagudo-Mendoza A, Arroyo L, Álvarez-Dávila E, et al. 2018. Compositional response of Amazon forests to climate change. *Global Change Biology* 25: 39–56.
- Esquivel-Muelbert A, Baker TR, Dexter KG, Lewis SL, ter Steege H, Lopez-Gonzalez G, Mendoza AB, Brienen R, Feldpausch TR, Pitman N et al. 2017. Seasonal drought limits tree species across the Neotropics. *Ecography* 40: 618–629.
- Fauset S, Johnson MO, Gloor M, Baker TR, Monteagudo A, Brienen RJW, Feldpausch TR, Lopez-Gonzalez G, Malhi Y, ter Steege H et al. 2015. Species contributions to stems, biomass and productivity in Amazon inventory plots. Hyperdominance in Amazonian forest carbon cycling. Nature Communications 6: 6857.
- Fisher RA, Muszala S, Verteinstein M, Lawrence P, Xu C, McDowell NG, Knox RG, Koven C, Holm J, Rogers BM *et al.* 2015. Taking off the training wheels: the properties of a dynamic vegetation model without climate envelopes, CLM4.5(ED). *Geoscientific Model Development* 8: 3593–3619.
- Friedlingstein P, Cox P, Betts R, Bopp L, von Bloh W, Brovkin V, Cadulee P, Doneyf S, Ebyg M, Fungh I et al. 2006. Climate—carbon cycle feedback analysis: results from the (CMIP)-M-4 model intercomparison. *Journal of Climate* 19: 3337–3353.
- Fu R, Yin L, Li W, Arias PA, Dickinson RE, Huang L, Chakraborty S, Fernandes K, Liebmann B, Fisher R et al. 2013. Increased dry-season length over southern Amazonia in recent decades and its implication for future climate projection. Proceedings of the National Academy of Sciences, USA 110: 18110– 18115.
- Garnier E, Cortez J, Billès G, Navas ML, Roumet C, Debussche M, Gérard L, Blanchard A, Aubry D, Neill C *et al.* 2004. Plant functional markers capture ecosystem properties during secondary succession. *Ecology* 85: 2630–2637.
- Gentine P, Guérin M, Uriarte M, Mcdowell NG, Pockman WT. 2016. An allometry-based model of the survival strategies of hydraulic failure and carbon starvation. *Ecohydrology* 9: 529–546.
- van Genuchten MT. 1980. A closed-form equation for predicting the hydraulic conductivity of unsaturated soils. Soil Science Society of America Journal 44: 892–898.
- Good P, Jones C, Lowe J, Betts R, Booth B. 2011. Quantifying environmental drivers of future tropical forest extent. *Journal of Climate* 24: 1337–1349.
- Grant PR, Grant BR, Huey RB, Johnson MTJ, Knoll AH, Schmitt J. 2017.
  Evolution caused by extreme events. Philosophical Transactions of the Royal Society of London. Series B: Biological Sciences 372: 20160146.
- Huntingford C, Zelazowski P, Galbraith D, Mercado LM, Sitch S, Fisher R, Lomas M, Walker AP, Jones CD, Booth BBB et al. 2013. Simulated resilience of tropical rainforests to CO<sub>2</sub>-induced climate change. Nature Geoscience 6: 268–273.
- Hutyra LR, Munger JW, Nobre CA, Saleska SR, Vieira SA, Wofsy SC. 2005.
  Climatic variability and vegetation vulnerability in Amazônia. *Geophysical Research Letters* 32: L24712.
- Ivanov VY, Hutyra LR, Wofsy SC, Munger JW, Saleska SR, Oliveira RC Jr, Camargo PB. 2012. Root niche separation can explain avoidance of seasonal drought stress and vulnerability of overstory trees to extended drought in a mature Amazonian forest. Water Resources Research 48: W12507.
- Jiménez-Muñoz JC, Mattar C, Barichivich J, Santamaría-Artigas A, Takahashi K, Malhi Y, Sobrino JA, van der Schrier G. 2016. Record-breaking warming and extreme drought in the Amazon rainforest during the course of El Niño 2015–2016. Scientific Reports 6: 33130.
- Joetzjer E, Delire C, Douville H, Ciais P, Decharme B, Fisher R, Christoffersen B, Calvet JC, da Costa ACL, Ferreira L et al. 2014. Predicting the response of the Amazon rainforest to persistent drought conditions under current and future climates: a major challenge for global land surface models. Geoscientific Model Development 7: 2933–2950.

- Konings AG, Williams AP, Gentine P. 2017. Sensitivity of grassland productivity to aridity controlled by stomatal and xylem regulation. *Nature Geoscience* 7: 2193–2197.
- Levine NM, Zhang K, Longo M, Baccini A, Phillips OL, Lewis SL, Alvarez-Dàvila E, Andrade ACG, Brienen RJW, Erwin TL et al. 2016. Ecosystem heterogeneity determines the ecological resilience of the Amazon to climate change. Proceedings of the National Academy of Sciences, USA 113: 793–797.
- Lin YS, Medlyn BE, Duursma RA, Prentice IC, Wang H, Baig S, Eamus D, Dios VR, Mitchell P, Ellsworth DS *et al.* 2015. Optimal stomatal behavior around the world. *Nature Climate Change* 5: 459–464.
- Lintner BR, Biasutti M, Diffenbaugh NS, Lee J-E, Niznik MJ, Findell KL. 2012. Amplification of wet and dry month occurrence over tropical land regions in response to global warming. *Journal of Geophysical Research* 117: D11106.
- Longo M. 2013. Amazon forest response to changes in rainfall regime: results from an individual-based dynamic vegetation model. PhD Thesis: Harvard University, Cambridge, MA, USA.
- Malhi Y, Aragăo LE, Galbraith D, Huntingford C, Fisher R, Zelazowski P, Sitch S, McSweeney C, Meir P. 2009. Exploring the likelihood and mechanism of a climate-change-induced dieback of the Amazon rainforest. *Proceedings of the National Academy of Sciences, USA* 106: 20610–20615.
- Manoli G, Ivanov VY, Fatichi S. 2018. Dry-season greening and water stress in Amazonia: the role of modeling leaf phenology. *Journal of Geophysical Research* 123: 1909–1926.
- Markesteijn L, Poorter L, Bongers F, Paz H, Sack L. 2011. Hydraulics and life history of tropical dry forest tree species: coordination of species' drought and shade tolerance. *New Phytologist* 191: 480–495.
- McDowell N, Pockman WT, Allen CD, Breshears DD, Cobb N, Kolb T, Plaut J, Sperry J, West A, Williams DG *et al.* 2008. Mechanisms of plant survival and mortality during drought: Why do some plants survive while others succumb to drought? *New Phytologist* 178: 719–739.
- Medlyn BE, De Kauwe MG, Duursma RA. 2016. New developments in the effort to model ecosystems under water stress. *New Phytologist* 212: 5–7.
- Meinzer FC, Johnson DM, Lachenbruch B, McCulloh KA, Woodruff DR. 2009. Xylem hydraulic safety margins in woody plants: coordination of stomatal control of xylem tension with hydraulic capacitance. *Functional Ecology* 23: 922–930.
- Nepstad DC, de Carvalho CR, Davidson EA, Jipp PH, Lefebvre PA, Negreiros GH, Silva ED, Stone TA, Trumbore SE, Vieira S. 1994. The role of deep roots in the hydrological and carbon cycles of Amazonian forests and pastures. *Nature* 372: 666–669.
- Nepstad DC, Tohver IM, Ray D, Moutinho P, Cardinot G. 2007. Mortality of large trees and lianas following experimental drought in an Amazon Forest. *Ecology* 88: 2259–2269.
- Oliveira RS, Costa FRC, Baalen E, Jonge A, Bittencourt PR, Almanza Y, Barros FV, Cordoba EC, Fagundes MV, Garcia S et al. 2019. Embolism resistance drives the distribution of Amazonian rainforest tree species along hydrotopographic gradients. New Phytologist 221: 1457–1465.
- Oliveira RS, Dawson TE, Burgess SSO, Nepstad DC. 2005. Hydraulic redistribution in three Amazonian trees. *Oecologia* 145: 354–363.
- Oyama MD, Nobre CA. 2003. A new climate–vegetation equilibrium state for Tropical South America. *Geophysical Research Letters* 30: 2199.
- Pammenter NW, Vander Willigen C. 1998. A mathematical and statistical analysis of the curves illustrating vulnerability of xylem to cavitation. *Tree Physiology* 18: 589–593.
- Panisset JS, Libonati R, Gouveia CMP, Machado-Silva F, França DA, França JRA, Peres LF. 2018. Contrasting patterns of the extreme drought episodes of 2005, 2010 and 2015 in the Amazon Basin. *International Journal of Climatology* 38: 1096–1104.
- Parrotta JA, Francis JK, DeAlmeida RR. 1995. *Trees of the Tapajo's: A photographic field guide.* Gen. Tech. Rep. IITF-1, US Department of Agricculture, Rio Piedras, Puerto Rico.
- Pereira L, Bittencourt PRL, Oliveira RS, Junior MBM, Barros FV, Ribeiro RV, Mazzafera P. 2016. Plant pneumatics: stem air flow is related to embolism new perspectives on methods in plant hydraulics. *New Phytologist* 211: 357–370.
- Phillips OL, van der Heijden G, Lewis SL, López-González G, Aragão LEOC, Lloyd J, Malhi Y, Monteagudo A, Almeida S, Dávila EA et al. 2010. Drought mortality relationships for tropical forests. New Phytologist 187: 631–646.

- Pockman WT, Sperry JS. 2000. Vulnerability to xylem cavitations and the distribution of Sonoran Desert vegetation. American Journal of Botany 87: 1287–1299.
- Pyle EH, Santoni GW, Nascimento HEM, Hutyra LR, Vieira S, Curran DJ, van Haren J, Saleska SR, Chow VY, Camargo PB. 2008. Dynamics of carbon, biomass, and structure in two Amazonian forests. *Journal of Geophysical Research: Biogeosciences* 114: 1–20.
- R Core Team. 2018. R: a language and environment for statistical computing, v.3.5. Vienna, Austria: R Foundation for Statistical Computing. [WWW document] URL https://www.R-project.org/
- Restrepo-Coupe N, Levine NM, Christoffersen BO, Albert LP, Wu J, Costa MH, Galbraith D, Imbuzeiro H, Martins G, Araujo AC et al. 2016. Do dynamic global vegetation models capture the seasonality of carbon fluxes in the Amazon basin? A data-model intercomparison. Global Change Biology 23: 191–208.
- Rowland L, da Costa ACL, Galbraith DR, Oliveira RS, Binks OJ, Oliveira AAR, Pullen AM, Doughty CE, Metcalfe DB, Vasconcelos SS *et al.* 2015. Death from drought in tropical forests is triggered by hydraulics not carbon starvation. *Nature* 528: 119–122.
- Sakschewski B, von Bloh W, Boit A, Poorter L, Peña-Claros M, Heinke J, Joshi J, Thonicke K. 2016. Resilience of Amazon forests emerges from plant trait diversity. *Nature Climate Change* 6: 1032–1036.
- Schneider CA, Rasband WS, Eliceiri KW. 2012. NIH Image to ImageJ: 25 years of image analysis. Nature Methods 9: 671–675.
- Scholz A, Klepsch M, Karimi Z, Jansen S. 2013. How to quantify conduits in wood? *Frontiers in Plant Science* 4: 56.
- Sperry JS, Donnelly JR, Tyree MT. 1988. A method for measuring hydraulic conductivity and embolism in xylem. *Plant, Cell & Environment* 11: 35–40.
- Sperry JS, Hacke UG, Oren R, Comstock JP. 2002. Water deficits and hydraulic limits to leaf water supply. *Plant, Cell & Environment* 25: 251–263.
- Sperry JS, Love DM. 2015. What plant hydraulics can tell us about responses to climate-change droughts. *New Phytologist* 207: 14–27.
- Ter Steege H, Pitman NCA, Sabatier D, Baraloto C, Salomao RP, Guevara JE, Philips OL, Castilho CV, Magnusson WE, Molino JF *et al.* 2013. Hyperdominance in the Amazonian Tree Flora. *Science* 342: 1243092.
- Trueba S, Pouteau R, Lens F, Feild TS, Isnard S, Olson ME, Delzon S. 2017. Vulnerability to xylem embolism as a major correlate of the environmental distribution of rain forest species on a tropical island. *Plant, Cell & Environment* 40: 277–289.
- Tyree MT, Sperry JS. 1989. Vulnerability of xylem to cavitation and embolism. Annual Review of Plant Physiology and Plant Molecular Biology 40: 19–38.
- Vieira S, de Camargo PB, Selhorst D, da Silva R, Hutyra L, Chambers JQ, Brown IF, Higuchi N, dos Santos J, Wofsy SC et al. 2004. Forest structure and carbon dynamics in Amazonian tropical rain forests. *Oecologia* 140: 468–479.
- Williamson GB, Laurance WF, Oliveira AA, Delamônica P, Gascon C, Lovejoy TE, Pohl L. 2000. Amazonian tree mortality during the 1997 El Niño drought. Conservation Biology 14: 1538–1542.
- Xu X, Medvigy D, Powers JS, Becknell JM, Guan K. 2016. Diversity in plant hydraulic traits explains seasonal and inter-annual variations of vegetation dynamics in seasonally dry tropical forests. *New Phytologist* 212: 80–95.

# **Supporting Information**

Additional Supporting Information may be found online in the Supporting Information section at the end of the article.

Fig. S1 Times series of climatic and hydrologic variables for the studied sites.

- Fig. S2 Soil water content time series for the studied sites.
- **Fig. S3** Relationship between monthly mean canopy conductance and residuals of vapour pressure deficit and cumulative water deficit for the studied sites.
- **Fig. S4** The relationship between monthly mean evapotranspiration and vapour pressure deficit and cumulative water deficit for the studied sites.
- Methods S1 Species dominance and trait distribution in the communities.
- **Methods S2** The biogeographic dry affiliation index as a trait to distinguish LSF and HSF community composition.
- Methods S3 Eddy covariance flux measurements.
- Methods S4 Canopy conductance calculation
- Methods S5 Statistic functions and packages
- **Table S1** List of species names, family and mean hydraulic trait values for all studied species at low seasonal forest (LSF) and high seasonal forest (HSF).
- **Table S2** Summary of hydraulic traits and statistical results of hypothesis 1, that HSF has more drought-resistant hydraulic traits than LSF.
- **Table S3** General mixed model result from the test of hypothesis 2, that species from HSF are less sensitive to ENSO than species from LSF.
- **Table S4** General mixed model result from the test of our hypothesis 3, that HSF is less sensitive to atmospheric drought and soil drought than the LSF.
- **Table S5** General mixed site-specific model results for evapotranspiration (ET) varying in function of atmospheric drought and soil drought.

Please note: Wiley Blackwell are not responsible for the content or functionality of any Supporting Information supplied by the authors. Any queries (other than missing material) should be directed to the *New Phytologist* Central Office.

# New Phytologist Supporting Information

Article title: Hydraulic traits explain differential responses of Amazonian forests to the 2015 El Nino -induced drought

Authors: Fernanda V. Barros, Paulo R. Bittencourt, Mauro Brum, Natalia Restrepo-Coupe, Luciano Pereira, Grazielle S. Teodoro, Scott Saleska, Laura S. Borma, Bradley O. Christoffersen, Deliane Penha, Luciana F. Alves, Adriano J.N. Lima, Vilany M.C. Carneiro, Pierre Gentine, Jung-Eun Lee, Leila S. M. Leal, Alessandro C. Araujo, Luiz E. O. C. Aragão, Valeriy Ivanov, Rafael S. Oliveira.

Article acceptance date: Click here to enter a date.

# The following Supporting Information is available for this article

**Table S1.** List of species name, family and mean hydraulic traits value for all studied species at low seasonal forest (LSF) and high seasonal forest (HSF).

**Table S2.** Summary of hydraulic traits and statistical results of hypothesis 1, that HSF has more drought resistant hydraulic traits than LSF.

**Table S3.** General mixed model result from the test of hypothesis 2, that species from HSF are less sensitive to ENSO than species from LSF.

**Table S4.** General mixed model result from the test of our hypothesis 3, that HSF forest is less sensitive to atmospheric drought and soil drought than the LSF forest.

**Table S5.** General mixed site-specific model results for evapotranspiration (ET) varying in function of atmospheric drought, soil drought.

Methods S1 Species dominance and trait distribution in the communities.

**Methods S2.** The biogeographic dry affiliation index as a trait to differ LSF and HSF community composition.

**Methods S3** Eddy covariance flux measurements.

Methods S4 Canopy conductance calculation.

Methods S5 Statistic functions and packages

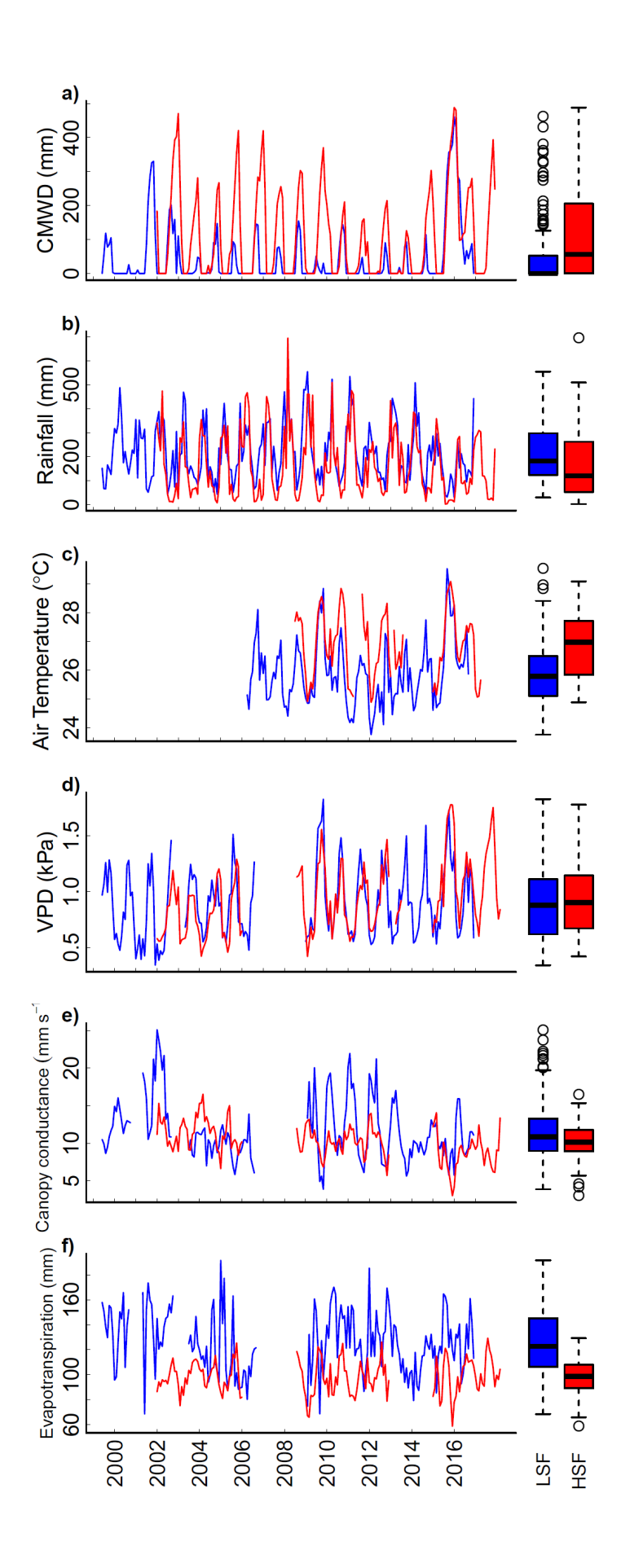
**Figure S1.** Times series of (a) cumulative water deficit (CMWD; mm); (b) rainfall (mm); (c) air temperature (°C); (d) vapour pressure deficit (VPD; kPa); (e) canopy conductance (mm s<sup>-1</sup>); and (f) evapotranspiration (mm); for the low seasonality forest (LSF, Manaus, blue) and the high seasonality forest (HSF, Tapajos, red). Boxes are the data distribution of the time series for LSF and HSF. Whiskers in a) are either maximum/minimum value or, when outliers are present, 1.5 interquartile range above/bellow the quartiles 2 and 3.

**Figure S2.** Monthly mean soil water content (%) as a function of monthly cumulative water deficit (CMWD; mm) for (a) low seasonality forest (LSF, Manaus) and, (b) high seasonality forest (HSF, Tapajos). Soil water content time series, available for (c) LSF in 2015 and, (d) HSF. Red lines are the soil water content at a depth of 0.8m for LSF and 0.5m for HSF, green lines are 1.6m in LSF and 1m in HSF and blue line is 2.4m in LSF and 2m in HSF. Black lines in (a) and (b) are the best-fit linear model for LSF (F (1,9) = 25.6;  $r^2 = 0.74$ ; p < 0.001) and HSF (F (1,52) = 154.5;  $r^2 = 0.75$ ; p < 0.001). Soil water content data was not calibrated, so while patterns are reliable, absolute values should be evaluated with care.

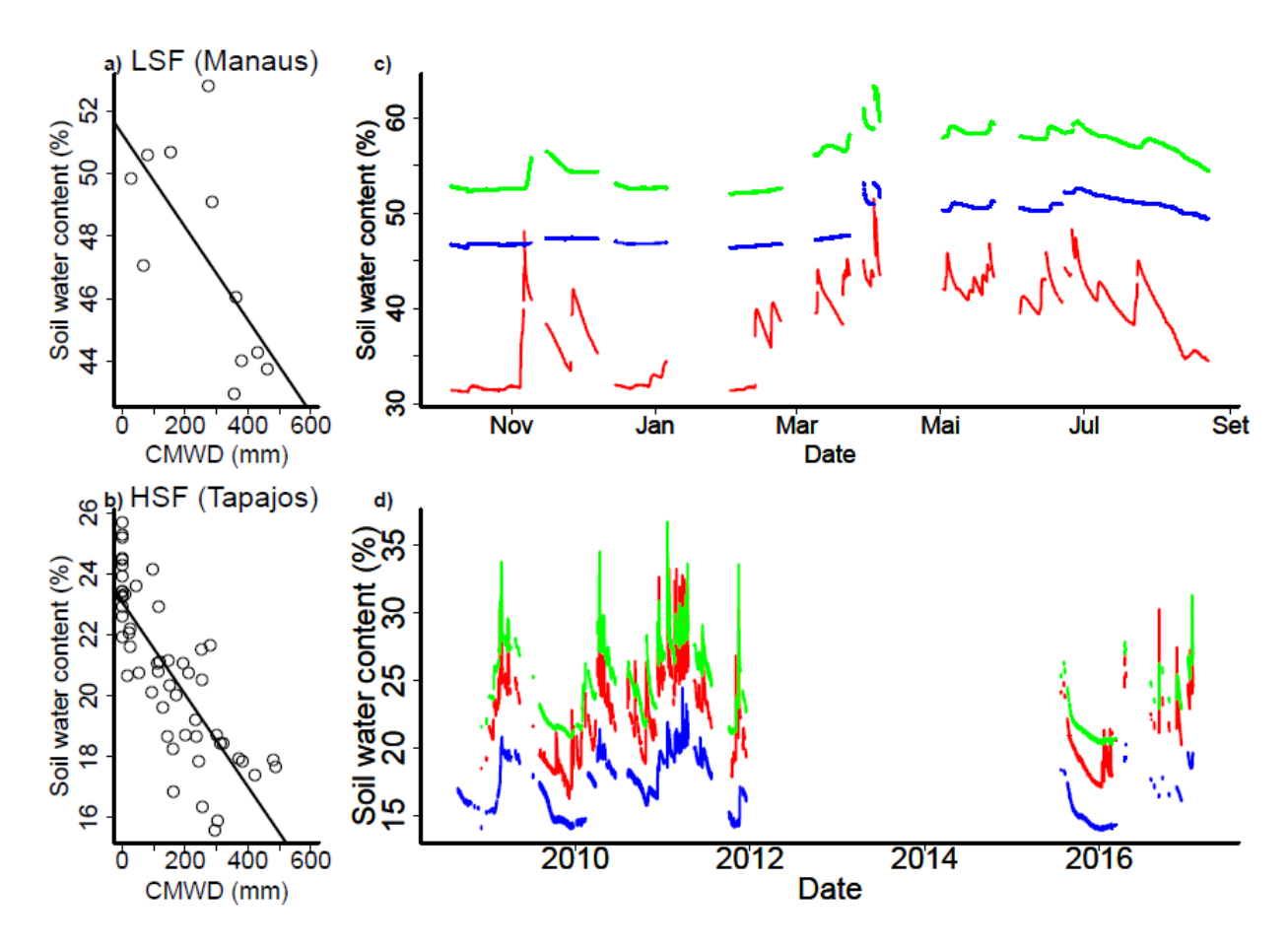
**Figure S3.** The relationship between monthly mean canopy conductance (G<sub>S</sub>) and CMWD<sub>r</sub> in the (a) low seasonality forest (LSF, Manaus), and (b) high seasonality forest (HSF, Tapajos); and canopy conductance (Gs) and VPD<sub>r</sub> for (c) LSF and (d) HSF. The CMWD<sub>r</sub>, and VPD<sub>r</sub> correspond to the residuals of monthly mean VPD (vapour pressure deficit) and monthly CMWD (cumulative water deficit) after removing the correlation between VPD and CMWD. The data correspond to the period from July to December. The colour of the data points is proportional to the VPD<sub>r</sub> value in plots (a) and (b) and to the CMWD<sub>r</sub> values in plots (c) and (d), according to the colour charts bellow the panels. Note both sites were modelled together and the p-value in panel (a) also applies to panel (b) and p and R<sup>2</sup>m values in panel (c) also apply to panel (d). Triangles points are data from 2015 ENSO. Circles points are monthly data from 1999 to 2016, excluding the 2015 ENSO period.

Figure S4. The relationship between monthly mean evapotranspiration (ET) and CMWD in the

(a) low seasonality forest (LSF, Manaus), and (b) high seasonality forest (HSF, Tapajos); and evapotranspiration (ET) and VPD for (c) LSF and (d) HSF. The data correspond to the period from July to December. The colour of the data points is proportional to the VPD value in plots (a) and (b) and to the CMWD values in plots (c) and (d), according to the colour charts bellow the panels. Note both sites were modelled together and the p-value in panel (a) also applies to panel (b) and p and R<sup>2</sup>m values in panel (c) also apply to panel (d). Triangles are data from 2015 ENSO. Circles are monthly data from 1999 to 2016, excluding the 2015 ENSO period.



**Figure S1.** Times series of (a) cumulative water deficit (CMWD; mm); (b) rainfall (mm); (c) air temperature (°C); (d) vapour pressure deficit (VPD; kPa); (e) canopy conductance (mm s<sup>-1</sup>); and (f) evapotranspiration (mm); for the low seasonality forest (LSF, Manaus, blue) and the high seasonality forest (HSF, Tapajos, red). Boxes are the data distribution of the time series for LSF and HSF. Whiskers in a) are either maximum/minimum value or, when outliers are present, 1.5 interquartile range above/bellow the quartiles 2 and 3.



**Figure S2.** Monthly mean soil water content (%) as a function of monthly cumulative water deficit (CMWD; mm) for (a) low seasonality forest (LSF, Manaus) and, (b) high seasonality forest (HSF, Tapajos). Soil water content time series, available for (c) LSF in 2015 and, (d) HSF. Red lines are the soil water content at a depth of 0.8m for LSF and 0.5m for HSF, green lines are 1.6m in LSF and 1m in HSF and blue line is 2.4m in LSF and 2m in HSF. Black lines in (a) and (b) are the best-fit linear model for LSF (F (1,9) = 25.6;  $r^2 = 0.74$ ; p < 0.001) and HSF (F (1,52) = 154.5;  $r^2 = 0.75$ ; p < 0.001). Soil water content data was not calibrated, so while patterns are reliable, absolute values should be evaluated with care.

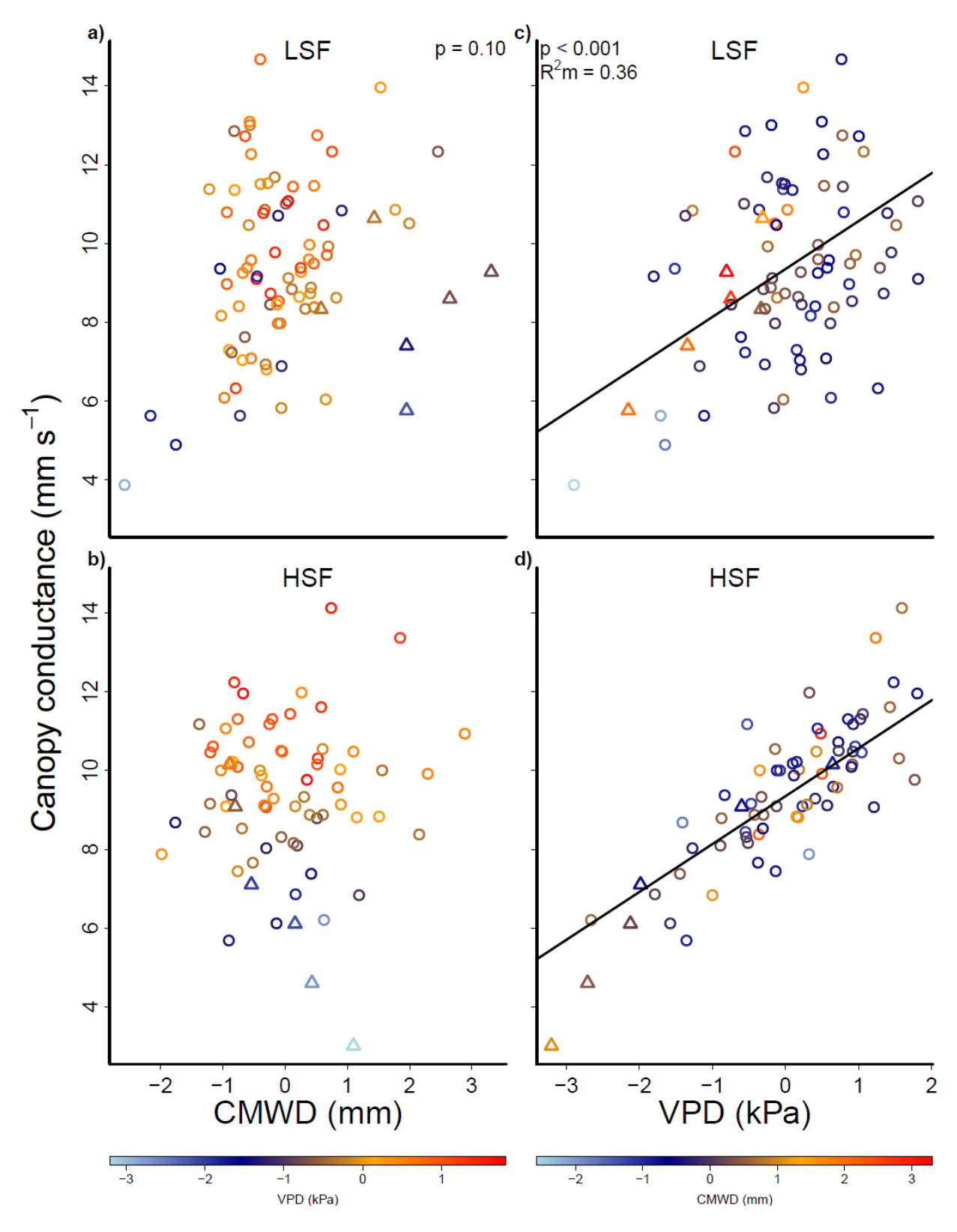


**Figure S3.** The relationship between monthly mean canopy conductance  $(G_S)$  and CMWD<sub>r</sub> in the (a) low seasonality forest (LSF, Manaus), and (b) high seasonality forest (HSF, Tapajos); and

canopy conductance (Gs) and VPD<sub>r</sub> for (c) LSF and (d) HSF. The CMWD<sub>r</sub>, and VPD<sub>r</sub> correspond to the residuals of monthly mean VPD (vapour pressure deficit) and monthly CMWD (cumulative water deficit) after removing the correlation between VPD and CMWD. The data correspond to the period from July to December. The colour of the data points is proportional to the VPD<sub>r</sub> value in plots (a) and (b) and to the CMWD<sub>r</sub> values in plots (c) and (d), according to the colour charts bellow the panels. Note both sites were modelled together and the p-value in panel (a) also applies to panel (b) and p and R<sup>2</sup>m values in panel (c) also apply to panel (d). Triangles points are data from 2015 ENSO. Circles points are monthly data from 1999 to 2016, excluding the 2015 ENSO period.

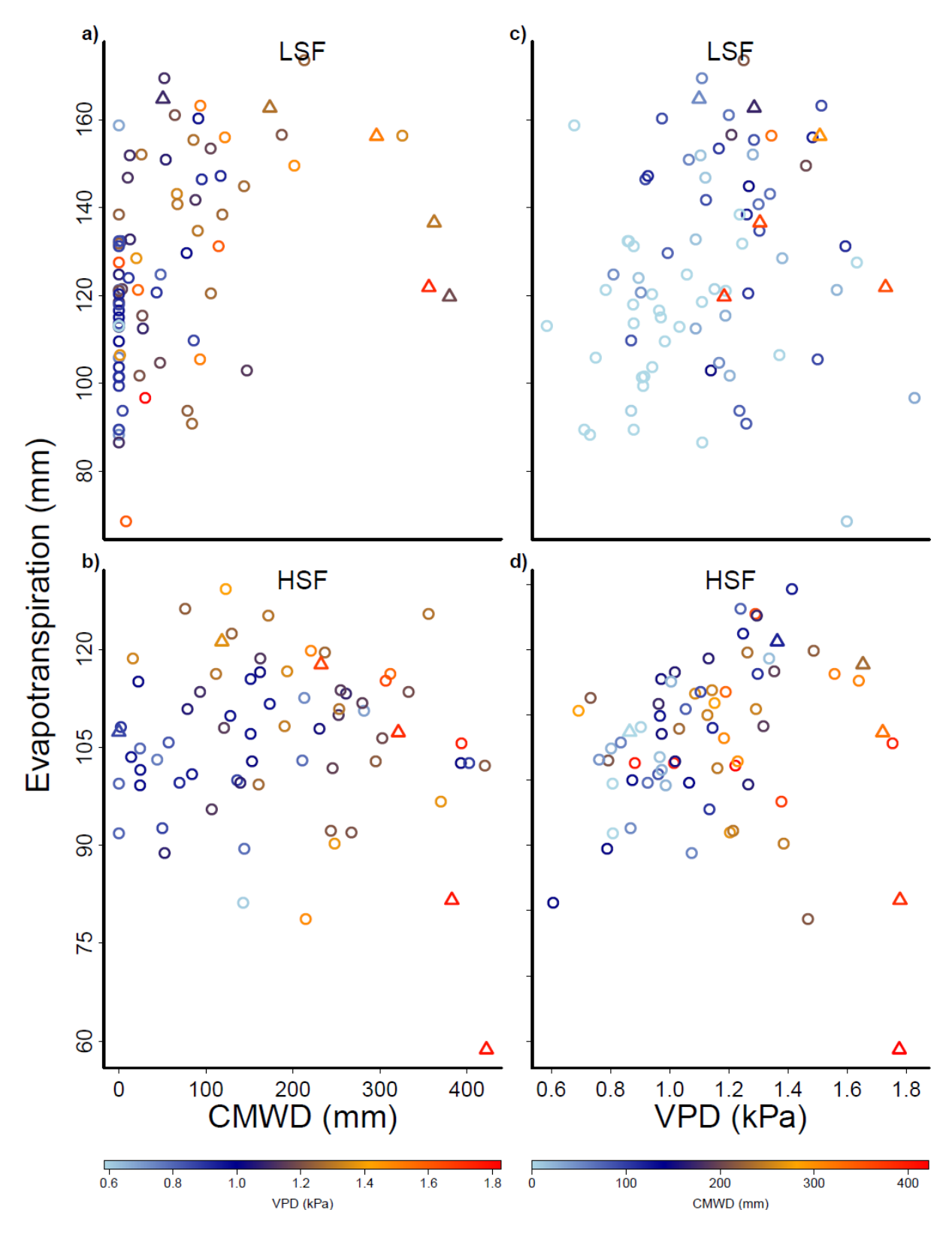


**Figure S4.** The relationship between monthly mean evapotranspiration (ET) and CMWD in the (a) low seasonality forest (LSF, Manaus), and (b) high seasonality forest (HSF, Tapajos); and

evapotranspiration (ET) and VPD for (c) LSF and (d) HSF. The data correspond to the period from July to December. The colour of the data points is proportional to the VPD value in plots (a) and (b) and to the CMWD values in plots (c) and (d), according to the colour charts bellow the panels. Note both sites were modelled together and the p-value in panel (a) also applies to panel (b) and p and R<sup>2</sup>m values in panel (c) also apply to panel (d). Triangles are data from 2015 ENSO. Circles are monthly data from 1999 to 2016, excluding the 2015 ENSO period.

**Table S1**. List of species name, family and mean hydraulic traits value for all studied species at low seasonal forest (LSF) and high seasonal forest (HSF). The traits abbreviations are described below (\*). The sample size (n) for the hydraulic traits evaluated in this study is represented for each species. NA indicates not available data.

Site	Species	Family	n	RD	Ψ50	Ψ88	$\Psi_{nonENSO}$	$\Psi_{ENSO}$	VD	VA	Kh	Dh
	Caryocar glabrum	Caryocaraceae	2	0.01	-1.78	-3.10	-0.71	-1.1	578.2	5.9	22.6	34.6
	Dypterix odorata	Fabaceae	2	0.14	-4.47	-6.22	-0.95	-2.61	285.6	13.2	6.5	30.1
	Eschweilera coriaceae	Lecitidaceae	4	1.77	-1.57	-1.59	-1.41	-1.54	465.8	8.2	10.6	30.1
	Eschweilera cyathiformis	Lecitidaceae	1	0.26	-3.05	-4.74	-0.8	-2.895	NA	NA	NA	NA
	Eschweilera sp.	Lecitidaceae	1	0.54	-2.47	-6.20	-1.71	-2.545	303.0	19.9	3.1	19.4
	Eschweilera wachenheimii	Lecitidaceae	2	3.02	-2.19	-2.86	-1.51	-1.59	337.4	12.1	7.7	29.3
	Goupia glabra	Celastraceae	3	1.2	-2.2	-3.80	-0.57	-1.14	495.2	7.6	16.7	31.0
	Gustavia elliptica	Lecitidaceae	3	0.09	-2.75	-6.64	-1.43	-1.63	890.6	6.2	5.1	20.8
LSF	Lecyths prancei	Lecitidaceae	3	0.76	-1.8	-2.13	-2.09	-1.93	384.2	10.0	9.5	30.2
	Maquira sclerophylla	Moraceae	3	0.24	-2.21	-3.82	-1.07	-1.72	773.5	5.9	15.8	26.5
	Minquartia guianensis	Olacaceae	2	1.21	-2.16	-4.56	-1.28	-1.8	611.2	11.1	2.0	16.3
	Ocotea sp.	Lauraceae	2	0.16	-1.84	-3.60	-0.91	-2.16	206.8	17.8	12.8	33.5
	Pouteria anomala	Sapotaceae	3	1.05	-1.01	-1.47	-0.9	-1.35	770.4	5.9	6.9	23.9
	Pouteria erythrochrysa	Sapotaceae	1	0.38	-3.92	-6.96	-0.88	-1.43	NA	NA	NA	NA
	Protium hebetatum	Burseraceae	3	0.64	-1.49	-3.52	-0.71	-1.16	697.9	8.5	5.8	19.3
	Scleronema micranthum	Bombacaceae	3	1.37	-1.77	-1.97	-1.16	-1.13	602.3	5.8	23.9	34.5
	Zygia racemosa	Fabaceae	3	0.85	-3.02	-6.19	-0.49	-1.16	188.1	27.6	3.5	23.0

	Amphyrrhox longifolia	Violaceae	5	1.08	-2.28	-5.77	-2.12	-1.93	1005.1	7.1	1.5	15.1
	Chamaecrista xinguensis	Fabaceae	3	6.15	-3.14	-6.05	-2.68	-2.58	300.5	11.4	9.7	32.9
	Coussarea albescens	Rubiaceae	3	4.61	-4.86	-6.64	-2.25	-3.21	1314.0	5.7	1.6	14.5
	Endopleura uchi	Humiriaceae	2	1.01	-1.52	-4.83	-1.1	-1.62	594.3	7.2	7.9	26.4
HSF	Erisma unsinatum	Vochysiaceae	3	11.07	-2.13	-3.24	-1.22	-1.06	391.7	11.2	5.6	26.5
	Manilkara huberi	Sapotaceae	3	26.96	-1.75	-4.51	NA	NA	NA	NA	NA	NA
пог	Mezilaurus itauba	Lauraceae	2	1.2	-2.98	-5.54	-1.64	-1.98	992.1	4.3	12.3	25.8
	Miconia lepidota	Melastomataceae	3	0.09	-5.02	-6.76	-1.96	-3.01	1337.1	4.9	4.0	18.1
	Minquartia guianensis	Olacaceae		0.06	-2.37	-6.03	NA	NA	NA	NA	NA	NA
	Protium apiculatum	Burseraceae	3	2.15	-1.94	-2.12	-1.38	-1.29	956.1	5.0	7.5	23.3
	Rinourea passourea	Violaceae	5	7.59	-2.99	-7.30	-2.58	-4.43	909.4	9.2	0.6	12.5
	Tachigali chrysophylla	Fabaceae	2	15.77	-3.79	-5.13	NA	NA	NA	NA	NA	NA

<sup>\*</sup> RD: relative dominance (percentage stem basal area of the species in relation to forest tree stem basal area),  $\Psi_{50}$  (MPa),  $\Psi_{88}$  (MPa),  $\Psi_{nonENSO}$ : minimum water potential for the non-ENSO year (MPa),  $\Psi_{ENSO}$ : minimum water potential for the ENSO 2015 (MPa), VD: Vessel density (number of vessels per mm² of xylem area), VA: Vessel area (percentage vessel area xylem area),  $K_h$ : Potential specific conductance (kg MPa<sup>-1</sup> s<sup>-1</sup> m<sup>-1</sup>),  $D_h$ : Hydraulic diameter ( $\mu$ )

**Table S2.** Summary of hydraulic traits and statistical results of hypothesis 1, that HSF has more drought resistant hydraulic traits than LSF: mean ( $\mu$ ), standard deviation (sd), Dominance Weighted mean (DWM) for each forest (LSF - low seasonal forest, HSF - high seasonal forest); and the statistical results of one tailed Welch's t-test to assess if mean traits from LSF species are less hydraulically resistant than HSF species (p value, df- degrees of freedom, t value).  $p_{dwm}$  is the p-value for the same hypothesis as tested by Welch's t-test, but testing whether the community level trait, estimated from DWM, differs between the two forests. The  $p_{dwm}$  is the result of a Monte Carlo method probability distribution with the test statistic being difference in the DWM trait between the two communities (see Analysis section for details). Values in bold represent significant differences at the 95% confidence level (p<0.05). The traits abbreviation is described on Table S1.

TF •4	LSF	(Mar	naus; K	(34)	HSI	F (Tap	oajos; K	(67)		Stat	tistics	
Traits	mean	sd	DWM	95%	mean	<u>sd</u>	DWM	95%	p	df	t	$p_{dwm}$
$\Psi_{50}$	-2.34	0.89	-2.07	0.34	-2.90	1.15	-2.78	0.65	0.09	19.72	1.42	0.058
$\Psi_{88}$	-4.08	1.83	-3.30	0.87	-5.33	1.49	-5.10	1.08	0.027	26.33	2.02	0.026
$\Psi_{50}$ - $\Psi_{88}$	1.74	1.2	1.22	0.61	2.43	1.2	2.32	0.84	0.07	23.7	-1.50	0.055
$\Psi_{nonENSO}$	-1.09	0.43	-1.20	0.23	-1.88	0.58	-1.96	0.55	0.002	12.80	3.59	0.030
$\Psi_{ENSO}$	-1.70	0.56	-1.55	0.22	-2.35	1.07	-2.44	1.11	0.06	10.39	1.69	0.122
$HSM_{P50}$	1.24	1.05	0.87	0.44	1.10	1.05	0.91	0.62	0.38	16.41	0.32	0.20
$HSM_{P88}$	2.99	1.95	2.10	0.97	3.48	1.32	3.25	1.07	0.77	22.24	-0.76	0.20
VD	506	220	476	100	867	369	692	309	0.011	11.48	-2.67	0.053
VA	11.04	6.35	10.87	3.25	7.35	2.69	9.22	2.09	0.031	20.44	1.98	0.18

$k_h$	10.16	6.87	9.76	3.69	5.64	4.05	4.99	3.06	0.027	22.00	2.03	0.17
$D_h$	26.8	6	27.1	3.2	21.7	7	22.4	6.5	0.04	15.09	1.86	0.18

Table S3. General mixed model result from the test of hypothesis 2 that species from HSF are less sensitive to ENSO than species from LSF. Model testing p values are the log likelihood significance test of the effect of removing the variable from model. Final significant model with its parameters are presented below model testing.  $\Psi_{min}$  is dry season minimum leaf water potential. (1|species) indicates species is a random fixed effect on intercept. R<sup>2</sup>m and R<sup>2</sup>c are, r

<b>Model testing</b>	Response	Predictor 1	<b>Predictor 2</b>	Interaction
	$\Psi_{min}$	ENSO	Site	ENSO: Site
p-value		< 0.001	0.003	0.57
inal model: Ψ <sub>min</sub>	$\sim$ ENSO + Site + $(1 s_1)$	pecies)		
	Parameter	Value	Standard error	
	Intercept	-1.12	0.15	-
	ENSO	-0.56	0.12	
	Site (HSF)	-0.72	0.23	
	Species	0.49		
	R <sup>2</sup> m	0.34		
	$R^2c$	0.68		
Model testing	Response	Predictor 1	Predictor 2	Interaction
	$\Psi_{min}$	VPD	Site	VPD: site

Model testing	Response	Predictor 1	Predictor 2	Interaction
	$\Psi_{min}$	VPD	Site	VPD: site
p-value		< 0.001	0.001	0.008

Final model:  $\Psi_{min} \sim VPD + Site + (1|species)$ 

Parameter	Value	Standard error	
Intercept	0.74	0.5	
VPD	-1.41	0.32	
Site (HSF)	-2.32	0.62	
Site (HSF): VPD	1.1	0.41	
Species	0.4		

$R^2m$	0.32	
$R^2c$	0.66	

Model testing	Response	Predictor 1	Predictor 2	Interaction
	$\Psi_{min}$	CWD	Site	CWD: Site
p-value		< 0.001	0.11	0.31

Final model:  $\Psi_{min} \sim ENSO + Site + (1|species)$ 

Parameter	Value	Standard error
Intercept	-0.99	0.17
CWD	-0.0025	0.000489
Species	0.48	
R <sup>2</sup> m	0.23	
$R^2c$	0.64	

**Table S4.** General mixed model result from the test of our hypothesis 3, that HSF forest is less sensitive to atmospheric drought and soil drought than the LSF forest. Model testing p-values are the log likelihood significance test of the effect of removing the variable from model. Final significant model with its parameters are presented below model testing. CMWD is cumulative water deficit (mm) and VPD is vapour pressure deficit (kPa). CMWD<sub>r</sub> are the residual of CMWD after removing the effect of VPD on it and VPD<sub>r</sub> are the residual of VPD after removing the CMWD effect on it. (1|Month) indicates month of the year is a random fixed effect on intercept. R<sup>2</sup>m and R<sup>2</sup>c are, respectively, marginal and conditional pseudo-R<sup>2</sup>. Sample number is 158 for all models.

	D.	D 11 4 4	D 11 4 2	T
Model testing	Response	Predictor 1	Predictor 2	Interaction
	VPD	CWD	Site	CWD: Site
p-value		< 0.001	0.002	0.50
Final model: VPD	$O \sim CWD + Site + (1 N)$	Month)		
	Parameter	Value	Standard error	
	Intercept	1.05	0.05	-
	ENSO	-0.0012	0.0001	
	Site (HSF)	-0.12	0.04	
	Month	0.11		
	$R^2m$	0.22		
	$R^2c$	0.38		

<b>Model testing</b>	Response	Predictor 1	Predictor 2	Interaction
	CWD	VPD	Site	VPD: site
p-value		< 0.001	< 0.001	0.57

Final model:  $CWD \sim VPD + Site + (1|Month)$ 

Parameter	Value	Standard error
Intercept	-144.9	37.9
VPD	186.4	28.6
Site (HSF)	113.0	13.4
 Month	43.6	
$R^2m$	0.40	
$R^2c$	0.53	

<b>Model testing</b>	Response	Predictor 1	Predictor 2	Interaction
	Gs	$VPD_r$	Site	VPD <sub>r</sub> : Site
p-value		< 0.001	0.95	0.34
Final model: Gs ~	$VPD_r + Site + (1 Mon$	th)		
	Parameter	Value	Standard error	
	Intercept	9.35	0.19	-
	$VPD_r$	-1.28	0.13	
	Month	0.34		
	$R^2m$	0.36		
	$R^2c$	0.39		
Model testing	Response	Predictor 1	Predictor 2	Interaction
Trower costing	$G_s$	$CWD_r$	Site	CWD <sub>r</sub> : Site
p-value	J	0.10	0.95	0.16
Final model: Gs ~	(1 Month)	0.10	0.73	0.10
i mai model. Gs	Parameter	Value	Standard error	
	-			-
	Intercept	9.35	2.04	
	Month	0.32		
	$R^2m$	0.00		
	$R^2c$	0.02		
Model testing	Response	Predictor 1	Predictor 2	Interaction
Wiodel testing	$G_s$	VPD	Site	VPD: site
p-value	- 3	< 0.001	0.91	0.08
Final model: CW	$D \sim VPD + (1 Month)$			
	Parameter	Value	Standard error	
	Intercept	15.11	0.61	-
	VPD	-5.08	0.52	
	Month	0.22		
	$R^2m$	0.40		
	$R^2c$	0.42		

**Table S5.** General mixed site-specific model results for evapotranspiration (ET) varying in function of atmospheric drought, soil drought. Model testing p-values are the log likelihood significance test of the effect of removing the variable from model. Final significant model with its parameters are presented below model testing. CMWD is cumulative water deficit (mm) and VPD is vapour pressure deficit (kPa). CMWD<sub>r</sub> are the residual of CMWD after removing the effect of VPD on it and VPD<sub>r</sub> are the residual of VPD after removing the CMWD effect on it. (1|Month) indicates month of the year is a random fixed effect on intercept. R<sup>2</sup>m and R<sup>2</sup>c are, respectively, marginal and conditional pseudo-R<sup>2</sup>. For all models sample number is 154.

<b>Model testing</b>	Response ET	Predictor 1 VPDr	Predictor 2 Site	Interaction VPDr: Site
p-value		0.32	< 0.001	0.38
Final model: ET ~	Site $+ (1 Month)$			
	Parameter	Value	Standard error	
	Intercept	127.0	3.14	
	Site	-21.0	2.95	
	Month			
	$R^2m$	0.23		
	$R^2c$	0.31		

Model testing	Response	Predictor 1	Predictor 2	Interaction
	ET	$CMWD_r$	Site	$CMWD_r$ : Site
p-value		0.29	< 0.001	0.39
Final model: ET ~	Site + (1 Month)			
	Parameter	Value	Standard error	
	Intercept	127.0	3.14	
	Site	-21.0	2.95	
	Month			
	$R^2m$	0.23		
	$R^2c$	0.31		

**Methods S1.** Species dominance and trait distribution in the communities.

The low seasonal forest (LSF) and the high seasonal forest (HSF) differ in species dominance homogeneity, as described in the main text. The consequence of such difference in our sampling was an unbalance species sampling number and the total basal area correspondent: while in LSF we sampled 17 species, which correspond to 13.7% of this forest basal area, in HSF, only 9 species had a greater representation in the community, 35% of total basal area. The low representability in basal area of the LSF is here discussed in terms of whether the community-weighted mean could be used to represent the LSF community (the properties of community weighted mean), and whether an increase in our sampling size (i.e., including mores species) would change the results here presented (if there are no changes in our estimates when a larger data sample is considered). In this case we used the data set published by Oliveira et al. 2018, to show that traits are randomly distributed across species at this community.

Community-weighted mean (CWM) is a way to scale species trait for a community by weighting the trait for its representativeness, in terms of biomass, basal stem area, or another index. Estimation of CWM usually requires high coverage of the biomass or basal area of species in a community. However, community-weighted means only differ significantly from regular, non-weighted, community means when: (1) few species dominate the stand and their trait value differs from the community (non-weighted) mean. In this situation, CWM is biased towards dominant species and non-weighted means are more likely to differ from CWM; (2) or there is no dominant species (i.e. when situation (1) does not occur) but there is a relationship between species dominance and the trait evaluated. For example, suppose wood density increase with dominance (i.e. rarer species have denser wood). In this case, the traits of the more dominant species are different from the rare species. In a non-weighted community mean, random sampling of species would equally consider the traits of rare and dominant species, however dominant species have a distinct different trait value from those of rare species, making CWM and non-weighted mean differ.

To exemplify case 1), consider a community with 100 species, each with trait  $X \sim N$  (10,10). This community has a dominance  $D \sim \text{Beta}$  ( $\alpha$ ,  $\beta$ ), where 000.1 <=  $\alpha$ ,  $\beta$  <= 10. The Beta distribution can have both positive and negative skewness depending on the values of its parameters and changing its  $\alpha$  and  $\beta$  parameters generate a range of dominance distributions with

different skewness. For this simulated community, we generated its dominance and trait X value according to the above definitions 100000 times and calculate trait X is CWM and non-weighted mean, as well as the cumulative dominance of the five most dominant species (CD5) (Figure a).

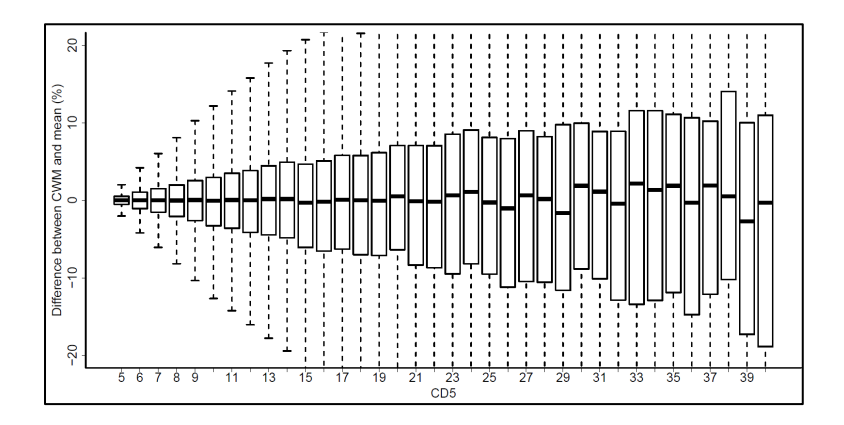


Figure a. Difference between community-weighted mean (CWM) and the non-weighted mean (expressed as a percentage of true CWM), as a function of five most dominant species (CD5) for all simulations.

This figure illustrates how the CWM is most likely to differ from the mean the more the weighting is dominated by a few species. The more the CWM is independent from a few species, the more likely it will be equal to the non-weighted community mean, which can be reasonably estimated from the mean of a subsample. As for the low seasonality forest (LSF), the cumulative dominance of the five dominant species is 10.7%, which suggests CWM is not much different from the regular community mean, as no single species, even if it is an outlier in the analysed trait, would heavily bias the CWM towards its value.

The above example presents a situation where  $X \sim N$  (10,10), that is, the standard deviation equals the mean. In the LSF we studied, P50 equals -2.34 ± 0.89 MPa and the standard deviation is 0.38 the mean. Using those values for trait X, and repeating the calculations above, the lower the variability of a trait, the less the CWM differs from the community regular mean, as there is less variability in total in the trait (i.e. it is less likely that a combination of a trait outlier species also is a dominant species) (Figure b).

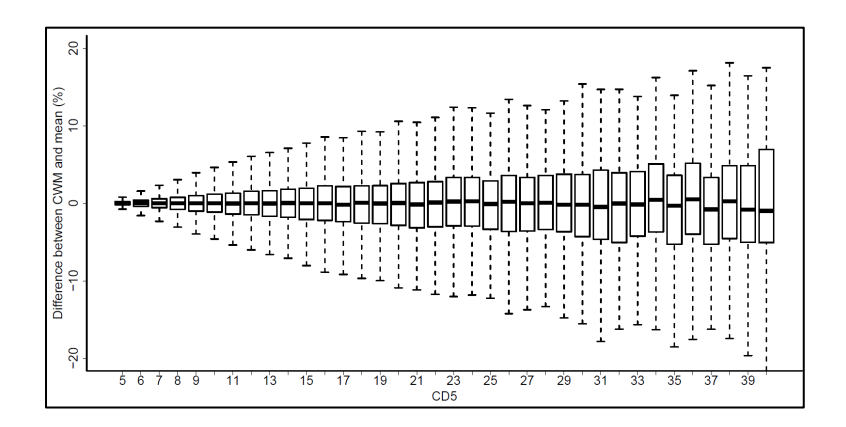


Figure b. Difference between community weighted mean (CWM) and the non-weighted mean (expressed as a percentage of true CWM) as a function of five most dominant species (CD5) for all simulations, for a trait with lower variability.

Finally, in Garnier et al. (2004), one of the key papers to first use CWM to infer ecosystem processes, the community with more species had a value of 12 species. Repeating the first procedure of Figure a, with trait  $X \sim N$  (10,10) and a total of 12 species is represented at Figure c. In this case, the CD5 cannot be lower than 42, the situation when the dominances are the most similar possible and when the CWM is most likely to equal the non-weighted mean (i.e. weighted mean equals non-weighted mean when all weights are equal). In the above situation, slightly more dominant species makes the CWM strongly differ from the community regular mean.

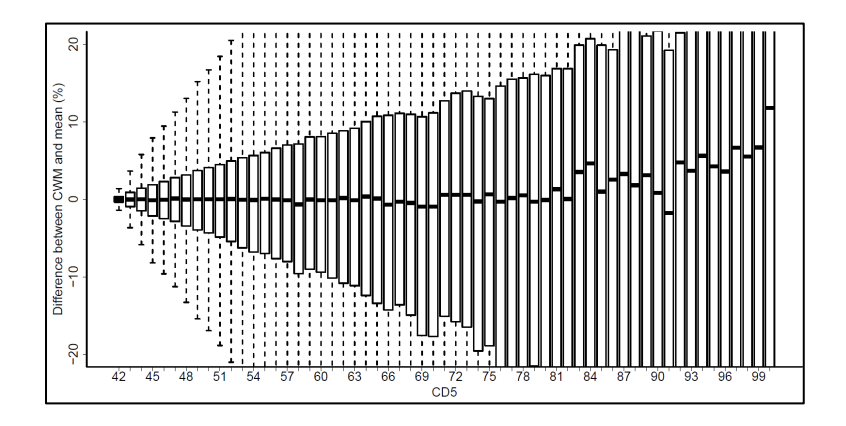


Figure c. Difference between community weighted mean (CWM) and the non-weighted mean (expressed as a percentage of true CWD) as a function of five most dominant species (CD5) for all simulations. Repeating the first procedure, with trait  $X \sim N$  (10,10) and a total of 12 species.

In summary, for case (1), we want to highlight that in rich communities where no few species dominate, the CWM and the community mean are unlikely to differ, particularly if the standard deviation of the trait being analysed is low compared to its mean. This is the case for the LSF, which is why we believe our coverage of 13% of the dominance, but 17 species, is a good indicator of the ecosystem function.

Regarding case (2), there is another situation when CWM and the non-weighted mean of a community can differ even if the conditions highlighted in (1) are fulfilled (i.e. species rich community with low trait variability and no few dominant species). This condition is when there is a relationship between the trait analysed and the dominance of the species. Applying the same analysis done before, lets consider the trait value of each species X = Da + N(10,5), where D is the dominance (D ~ Beta ( $\alpha$ ,  $\beta$ ), again) and a represents the intensity of the relationship between dominance and trait X. For a community with 100 species and no very dominant species (CD5 <= 10), we have:

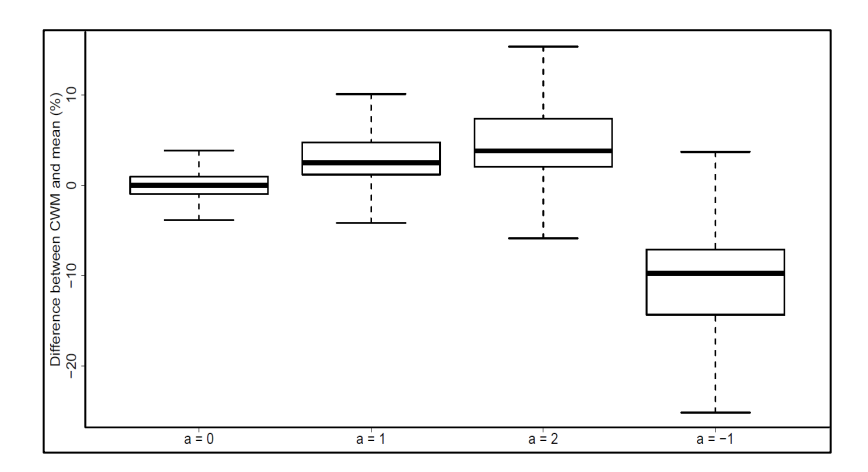


Figure d. Difference between community-weighted mean (CWM) and mean (%) for different situations of dependence between the trait and species dominance.

As can be seen, even for a situation with high trait variability ( $X \sim N$  (10,5)), if conditions pointed in (1) hold and dominance and the analysed trait is independent of dominance (a = 0), the difference between CWM and community mean is small. However, even if conditions highlighted in (1) hold, if the analysed trait is related to the dominance of the species, CWM and non-weighted community mean will systematically differ positively or negatively, depending on the whether the relationship between trait and dominance is positive or negative (Figure d). In our analysis, dominance is not related to any of the analysed traits for both, LSF or High

Seasonality Forest (HSF). Thus we conclude that, even if the community mean value we used for up scaling differs from the true CWM, it should not differ much.

Adding dataset of Ducke Reserve (Oliveira et al. 2018) to LSF measurements. The other topic of this method section includes the additional analysis showing that there is no change in our estimates when a larger data sample is considered. Here, we used the embolism data for Ducke Reserve at Manaus, Brazil (Oliveira et al. 2018), an area close to the studied LSF forest (~100 km distance), with the same climate and species composition. We paired this dataset with the species dominance in the LSF site, assuming the species trait is similar in both areas, to test whether increasing the basal area coverage would affect our traits estimative. The current dataset (n = 17, total dominance = 13.7%) has a mean P50 of -2.33 MPa (P50 CWM = -2.07 MPa). The larger database (n = 41, total dominance = 23.23%) has a mean P50 of -2.50 MPa (P50 CWM = -2.38 MPa) and it is not significantly different from the smaller dataset (T-test p = 0.47). According to this analysis, including more information is unlikely to change our results and conclusions.

Finally, we can say the LSF has very few dominant species, with the 5 most dominant species summing 10.67% of total basal area. To have a total basal area of 50% would require sampling at least the 53 most dominant species. We found no evidence that there is a relationship between relative dominance and the studied traits for LSF (linear model p = 0.57) (Figure e). Our data shows  $P_{50}$  in LSF is randomly distributed along species with different dominances. In this case, we can say the average is a good estimator of the community-weighted mean, which gives us confidence in our analysis.

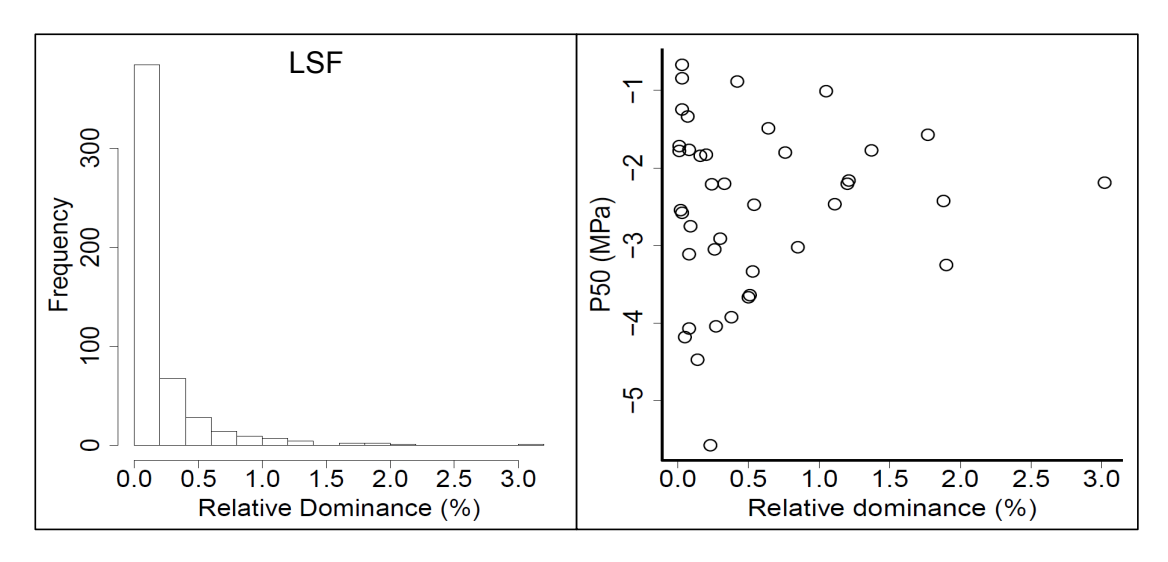


Figure e. Distribution of LSF dominance (left panel) and relationship between relative dominance and the studied traits (here showing P50; MPa) (right panel).

**Methods S2.** The biogeographic dry affiliation index as a trait to differ LSF and HSF community composition.

In addition to the evaluation of hydraulic trait to differ LSF and HSF communities, we used a new approach with the data published by Esquivel-Muelbert *et al.* (2017). In their study, the authors obtained an index, which considered the genus distribution across other Amazon sites, and represents the probability (p-value) of recording a higher dry-affiliated precipitation centre of gravity (PCG) value than the observed by chance for each different taxa (Esquivel-Muelbert *et al.*, 2017). Thus, if a certain genus has a p-value closer to zero, it meant it is nearly improbable to find another genus that has a higher dry-affiliation, indicating that the genus under consideration was found in drier environments. On the other hand, if a genus had a high p-value (closer to 1), it meant any other genus could have a higher dry-affiliation than it, indicating the genus under consideration is now found is wetter environments.

We used this dry-affiliation index (PCG 2-tail p-value) as a biogeographic trait of the genera. Figure 4a shows how this trait value was related with the gradient of CMWD across Amazonian sites (data from Esquivel-Muelbert *et al.* 2017). As lower is the genus PCG 2-tail p-value, higher is it's dry-affiliation, as it seems to occur in drier environments (higher water deficit - CWD). For each genus inventoried in our HSF and LSF communities, we obtained the respective dry affiliation index from Esquivel-Muelbert *et al.* (2017), and we extended this index as biogeographic trait for the entire community as suggested by Esquivel-Muelbert *et al.* (2018). Most of the studied species for LSF showed higher values of PCG 2-tail p-value, which is associated with low dry-affiliation and wet environments. The figure 4b shows this difference for the whole HSF and LSF community, we can see the lower dry-affiliation of LSF genera (higher PCG 2-tail p-value, p-value < 0.001), when compared with the HSF genera.

## **Methods S3.** Eddy covariance flux measurements.

The ET<sub>m</sub> was measured by the eddy-covariance method (Araújo et al., 2002; Restrepo-Coupe et

al., 2013). Tower observations, during the El Niño dry period, were of good quality with high continuity and daytime ET data completeness from September 2015 through March 2016 was 71.7 % at the K67 tower (HSF) and 63.4% at the K34 (LSF), from a total of 2544 daytime values. The data gaps were filled using the linear regression between incoming shortwave radiation (SW<sub>in</sub>; W m-2) and ET<sub>m</sub> observations by the eddy covariance tower ( $R^2 \sim 0.6$ , p<0.01) (Restrepo-Coupe et al., 2016). The ET-SWin relation is stably linear and consistent between dry and wet seasons at these sites (Hasler and Avissar, 2007). Although the relation between ET and SWin changes during extreme droughts, this did not significantly affect our analysis of ENSO because few points were filled by this method during the ENSO. Alternatively, we used satellite derived SW<sub>in</sub> (Shortwave Flux – All-Sky) from the Clouds and the Earth's Radiant Energy System (CERES) at 1-degree resolution for the 2003-2016 period (Kato et al., 2012; NASA, 2017b) and its relation to ET<sub>m</sub> monthly calculations to fill values when neither in situ fluxes or SWin were available. Any remaining missing ET<sub>m</sub> values (prior to 2003) were calculated as the mean monthly value from the available ET<sub>m</sub> measurements. Mean monthly precipitation was obtained from the Tropical Rainfall Measuring Mission (TRMM) 1999-2016 product (Huffman et al., 2007; NASA, 2017a). A single 0.25 x 0.25 degree cell was considered as representative of the study site.

# Methods S4. Canopy conductance calculation.

The G<sub>S</sub> was obtained by the inversion of the Penman–Monteith (PM) equation for daytime hours only:

$$ET = \frac{\epsilon.A + \left(\frac{c_p.\rho_a}{\gamma}\right)(e_s - e_a).G_a}{\epsilon + 1 + \left(\frac{G_a}{G_s}\right)}$$

where A is the available energy absorbed by the surface (W m<sup>-2</sup>), the net absorbed radiation minus the soil heat flux, here assumed to be equivalent to the sum of sensible and latent heat flux (H+LE);  $e_a$  is the actual vapour pressure (kPa),  $e_s$  is the saturation vapour pressure (kPa), (VPD= $e_s$  -  $e_a$ ),  $\gamma$  is the psychrometric coefficient (kPa °C<sup>-1</sup>),  $\rho_a$  is the mean air density (kg m<sup>-3</sup>),  $C_p$  is the specific heat of air at constant pressure (J kg<sup>-1</sup> °C<sup>-1</sup>),  $G_a$  and  $G_s$ , are the aerodynamic and surface conductance (m s<sup>-1</sup>), respectively; and  $\varepsilon$  is the unitless ratio between the slope of the saturation vapour pressure versus temperature curve (s; kPa °C<sup>-1</sup>) and  $\gamma$  ( $\varepsilon$  = s/ $\gamma$ ).

The canopy aerodynamic conductance ( $G_a$ ; m s<sup>-1</sup>) was calculated as the inverse of aerodynamic resistance ( $r_a$ ), which was calculated using the resistance to momentum transfer analogy and hence calculated with the expression proposed by Allen et al. (1998) and Verma (1989):

$$r_{a} = \frac{\ln\left(\frac{z-d}{z_{oH}}\right)}{ku^{*}} = \frac{1}{k^{2}u}\ln\left(\frac{z-d}{z_{o}}\right)\ln\left(\frac{z-d}{z_{oH}}\right)$$

$$G_a = \frac{1}{r_a}$$

where  $r_a$  is the aerodynamic resistance (s m<sup>-1</sup>),  $u^*$  is the friction velocity (m s<sup>-1</sup>), u the wind velocity (m s<sup>-1</sup>) measured at the EC height (z = 64 m at HSF and 52 m at LSF), d is the zero-plane displacement at  $z_0$  and  $z_{0H}$  are the roughness lengths for momentum and heat respectively (m). The quantities d,  $z_0$  and  $z_{0H}$  were estimated as d=2/3 h, 1/8 h and 1/80 h respectively, where h is canopy height (40 m).

The inversion of the Penman-Monteith equation implies that the available energy equals the sum of latent and sensible heat exchange (energy balance closure, EBC). As at most eddy covariance sites around the world, closure here is incomplete, typically around 80%, due in part to a mismatch between the footprints of the radiation and EC sensors, which is enhanced when low turbulence or advection is present (Leuning et al., 2012; Wilson et al., 2002) or by instrument malfunction (e.g. dirty net radiometer). We addressed this issue by removing monthly flux measurements for those periods when the total turbulent energy (LE and H) deviated from the overall linear regression estimate of LE + H *versus* R<sub>n</sub> by 3 standard deviations or more (Barraza et al., 2015). We calculated monthly values using the mean daily cycle of daytime hours for the period of aggregation to reduce the over/under sampling of certain times of day. On the monthly series we expect the energy storage terms (soil and air space between the EC and the surface) to approach to zero, thereby increasing the EBC.

# Methods S5 Statistic functions and packages

For all statistical analyses, data processing, and curve fitting, we used R (R Core Team 2018, version 3.5). We used the "t.test" function for the Welch's t-test (i.e. default of the function), which is more reliable than Student T-Test for samples of different sizes while not requiring variances of the two populations to be equal. We evaluated normality of the data using quantile-

quantile plots and the Shapiro-Wilk test ("shapiro.test" function). We used the "lm" function (base package) for general fixed linear models and the "lme" function ("nlme" package; Pinheiro *et al.* 2014) for general mixed effect models. We followed Zuur *et al.* (2009) and Thomas *et al.* (2017) guidelines for evaluating significance of model terms and validating models assumptions: i) we started with the more complex model and tested the importance of the terms evaluating whether dropping a term significantly affected the model using log-likelihood test with a threshold p value of 0.05; and ii) we evaluated the model assumptions (normality and homogeneity of residuals, collinearity of predictors and bias of influential measured) using diagnostic plots and sample cooks distance and dfbeta. We assessed mode performance using marginal and conditional pseudo-R<sup>2</sup> (R<sup>2</sup>m and R<sup>2</sup>c, calculate using "r.squaredGLMM" function from the "MuMIn" package; Barton 2016).

### References

Allen RG, Pereira LS, Raes D, Smith M, et al. 1998. Crop evapotranspiration- Guidelines for computing crop water requirements-FAO. *Irrigation and drainage* 300: 6541.

Araújo AC, Nobre AD, Kruijt B, Elbers JA, Dallarosa R, Stefani P, Randow C von, Manzi AO, Culf AD, Gash JHC, et al. 2002. Comparative measurements of carbon dioxide fluxes from two nearby towers in a central Amazonian rainforest: The Manaus LBA site. *Journal of Geophysical Research* 107: LBA 58-1–LBA 58-20.

**Barraza V, Restrepo-Coupe N, Huete A, Grings F, Van Gorsel E. 2015.** Passive microwave and optical index approaches for estimating surface conductance and evapotranspiration in forest ecosystems. *Agric. For. Meteorol.* **213**: 126–137.

**Barton K. 2016.** MuMIn: multi-model inference. https://cran.r-project.org/web/packages/MuMIn/index.html

Esquivel-Muelbert A, Baker TR, Dexter KG, Lewis SL, Brienen RJW, Feldpausch TR, et al. 2018. Compositional response of Amazon forests to climate change. Global Change Biology 25: 39-56.

Esquivel-Muelbert A, Baker TR, Dexter KG, Lewis SL, ter Steege H, Lopez-Gonzalez G, et al. 2017. Seasonal drought limits tree species across the Neotropics. *Ecography* 40: 618–629.

Garnier E, Cortez J, Billès G, Navas ML, Roumet C, Debussche M. *et al.* 2004. Plant Functional Markers Capture ecosystem properties during secondary succession. *Ecology* 85: 2630–2637.

**Hasler N, Avissar R**. **2007**. What Controls Evapotranspiration in the Amazon Basin? *Journal of Hydrometeorology* **8**: 380–395.

**Huffman GJ, Bolvin DT, Nelkin EJ, Wolff DB, Adler RF, Gu G et al. 2007.** The TRMM Multisatellite Precipitation Analysis (TMPA): Quasi-Global, Multiyear, Combined-Sensor Precipitation Estimates at Fine Scales. J. *Hydrometeorol.* **8**: 38–55.

Kato S, Loeb NG, Rose FG, Doelling DR, Rutan DA, Caldwell TE *et al.* 2012. Surface Irradiances Consistent with CERES-Derived Top-of-Atmosphere Shortwave and Longwave Irradiances. *J. Clim.* 26: 2719–2740.

**Leuning R, van Gorsel E, Massman WJ, Isaac PR. 2012.** Reflections on the surface energy imbalance problem. *Agric. For. Meteorol.* **156**: 65–74.

NASA 2017a. Tropical Rainfall Measuring Mission Project (TRMM), 3B43: Monthly 0.25x0.25 degree merged TRMM and other estimates v7 [WWW Document]. NASA Distrib Act. Arch Cent Goddard Space Flight Cent Earth Sci Greenbelt Md. URL http://mirador.gsfc.nasa.gov/cgi-bin/mirador/

**NASA, 2017b.** Clouds and the Earth's Radiant Energy System Information and Data (CERES) [WWW Document]. URL http://ceres.larc.nasa.gov/

Oliveira RS, Costa FRC, Baalen E, Jonge A, Bittencourt PR, Almanza Y et al. 2019. Embolism resistance drives the distribution of Amazonian rainforest tree species along hydrotopographic gradients. *New Phytologist* 221: 1457-1465.

**Pinheiro J, Bates D, DebRoy S, Sarkar D, R Core Team. 2014.** Nlme: Linear and Nonlinear Mixed Effects Models. R package version 3.1-118. http://CRAN.R-project.org/package=nlme.

Restrepo-Coupe N, da Rocha HR, Hutyra LR, da Araujo AC, Borma LS, Christoffersen B *et al.* 2013. What drives the seasonality of photosynthesis across the Amazon basin? A cross-site analysis of eddy flux tower measurements from the Brasil flux network. *Agricultural and Forest Meteorology* 182:128–144.

Restrepo-Coupe N, Levine NM, Christoffersen BO, Albert LP, Wu J, Costa MH, et al.

**2016.** Do dynamic global vegetation models capture the seasonality of carbon fluxes in the Amazon basin? A data-model intercomparison. *Glob. Change Biology* **23**:191-208.

**Thomas R, Lello J, Medeiros R, Pollard A, Robinson P, Seward A** *et al.* **2017.** Data analysis with R Statistical Software: a guidebook for scientists. Eco-Explore, United Kindgom.

**Verma SB. 1989**. Aerodynamic resistances to transfers of heat, mass and momentum. *Estim. Areal Evapotranspiration* **177**: 13–20.

Wilson K, Goldstein A, Falge E, Aubinet M, Baldocchi D, Berbigier P et al. 2002. Energy balance closure at FLUXNET sites. *Agric. For. Meteorol., FLUXNET 2000 Synthesis* 113: 223–243.

**Zuur A, Ieno E, Walker N, Saveliev A, Smith G. 2009.** *Mixed Effects Models and Extensions in Ecology with R.* New York, US. Springer Verlar.